A NUMERICAL INVESTIGATION
OF FLOW SEPARATION
ON A THREE-CALIBER TANGENT OGIVE

BY

LESLIE ANNE YATES

A DISSERTATION PRESENTED TO THE GRADUATE SCHOOL
OF THE UNIVERSITY OF FLORIDA IN PARTIAL FULFILLMENT
OF THE REQUIREMENTS FOR THE DEGREE OF DOCTOR OF PHILOSOPHY

UNIVERSITY OF FLORIDA

1986

To my mother and husband

ACKNOWLEDGMENTS

If it were not for the guidance and support of Professor Mark Clarkson and Dr. Gary Chapman, this work would not have been possible. When the results of my studies appeared to be inconclusive and contradictory, my discussions with Professor Mark Clarkson gave me new ideas and new approaches which enabled me to understand the results. I would especially like to thank Dr. Gary Chapman for his willingness to share his ideas, his questions which always got to the heart of the problem, and his suggestions which pointed out new directions of investigation.

This work was supported by a NASA Consortium agreement.

TABLE OF CONTENTS

Page

ACKNOWLEDGMENTS iii

ABSTRACT v

CHAPTERS

I INTRODUCTION 1

II TOPOLOGY AND SEPARATED FLOWS 8

III PARABOLIZED NAVIER-STOKES CODE 21

- Background 21
- Gridding 23
- Smoothing Coefficients 27

IV RESULTS AND DISCUSSION 29

- Comparison of Computational to Experimental Behavior 29
- Streamtubes 32
- Crossflow Information 35
- Tangential Separation 38
- Surface Information 39

V CONCLUSIONS 104

REFERENCES 106

BIOGRAPHICAL SKETCH 108

Abstract of Dissertation Presented to the Graduate School
of the University of Florida in Partial Fulfillment of the
Requirements for the Degree of Doctor of Philosophy

A NUMERICAL INVESTIGATION OF FLOW SEPARATION ON A THREE-CALIBER TANGENT OGIVE

By

Leslie Anne Yates

August, 1986

Chairman: Professor Mark Clarkson
Major Department: Engineering Sciences

Laminar solutions for crossflow separation on a three-caliber tangent ogive were computed with the parabolized Navier-Stokes code. Adaptations were made to the gridding scheme of the code to minimize oscillations and to improve the resolution of the solutions.

Solutions were obtained for Mach 2.0 at 10° and 15° angles of attack. For 10° the Reynolds numbers were chosen to be 12,000 and 300,000; for 15° the Reynolds numbers were 12,000 and 150,000. The limiting streamlines were calculated from the solutions. Convergence lines, lines upon which other limiting streamlines converged, were determined by visual inspection of the limiting streamline pattern. These convergence lines were shown not to be envelopes.

The dependency of the location of the convergence line upon the angle of attack and the Reynolds number agreed with experimental data. Also, the pressure distributions showed good agreement with available data.

There were no abrupt changes in the computed static pressure, pitot pressure, Mach number, vorticity, and skin friction that indicated where separation occurred.

The angle that the flow made with respect to the surface and the stretch, which was defined by the change in height of an infinitesimal streamtube at the surface, were studied. Again, there were no abrupt changes that indicated where separation occurred. The maximum values of the flow angle and stretch generally did not coincide with the convergence line or with each other.

The best indication of separation was given by the behavior of streamtubes that encircled the body. These streamtubes initially were chosen to lie well within the boundary layer. They developed bumps and then folds as the streamlines converged. These folds elongated, moved away from the body, and eventually rolled up.

These folds widened appreciably near the surface. This widening, along with the behavior of the other flow variables, made it impossible to define one separation line. Instead, separation appeared to involve extended regions of the flow.

CHAPTER I
INTRODUCTION

Considerable theoretical, experimental, and computational work has been undertaken in the last thirty years in an effort to understand the nature of three-dimensional separated flows. The introduction of topological theories that deal with the structure of continuous vector fields has facilitated the interpretation of these flows. It also has led to some disagreement between phenomenologists and topologists as to the preferred nomenclature and behavior of flow separation.

The phenomenological approach is represented by Wang's terminology and interpretation of three-dimensional flow separation.[1] Wang remarked that two types of separation can be observed experimentally. The first type, which he called open separation, develops gradually and results when the forces acting upon the fluid cause the streamlines to squeeze together and the fluid to be forced away from the surface. There are no sudden changes in the flow behavior when open separation begins, and its onset is not easily defined. The second type of separation, closed separation, does not result from a gradual process. Its existence and location are always defined by the presence of a saddle point in the limiting streamline pattern.

The topological approach of Tobak and Peake also led to two distinct classes of separation.[2,3] Tobak and Peake observed that, for one type of separation, the skin friction pattern for the separated flow can be continuously mapped onto the pattern for attached flow. This type of separation occurs when the streamlines converge and the fluid is forced off the surface. A second type of separation occurs when a saddle point is associated with the separation and the skin friction pattern for the separated flow cannot be continuously mapped onto the pattern for the attached flow. In keeping with the treatises on structural stability of Andronov et al.,[4,5] Tobak and Peake called these two classes of separation local and global, respectively.

These two approaches define the same two distinct classes of separation. Wang's open separation is essentially identical to Tobak and Peake's local separation; Wang's closed separation is essentially identical to Tobak and Peake's global separation. The two sets of definitions merely use different features of separated flow behavior for classification.

The difficulty with these two classification schemes is not in the classes of separation defined by the schemes, but in the terminology used to describe them. The terms global, local, open, and closed all have connotations that are not related to the strict mathematical definitions of Tobak and Peake or to the phenomenological descriptions of Wang. These connotations can be misleading and can color the interpretation of the flow behavior.

Another name for local (open) separation has been introduced by Chapman.[6] He noted that for local (open) separation there are no topological features on the body which indicate that separation has occurred. However, in the crossflow plane, a plane that is normal to the longitudinal axis of the body, all the topological characteristics of separation are observable. Because of this feature of local (open) separation, Chapman called this type of separation crossflow separation.

There are drawbacks with this definition as well. It is possible for the crossflow planes to show the topological characteristics of separation when no separation has occurred. Therefore, the presence of flow separation cannot be determined solely from examinations of crossflow planes. The three-dimensional character of the flow must also be examined in order to determine when and where separation has occurred. This aspect of the crossflow planes will be discussed further in Chapter IV.

Even with the drawbacks mentioned above, crossflow separation is perhaps the most desirable of the terms for separation without a saddle point. Crossflow separation is a separation which can be observed in a crossflow plane. It is not possible to identify this type of separation from the topology of the skin friction lines alone, nor does classifying it as a gradual process truly define it. Even when there is no saddle point associated with separation, the converging streamlines can squeeze together at a rate which will quickly force the fluid away from the surface. Hence, the term crossflow separation will be used in this study.

Although there is debate as to which terminology is preferable, there is a consensus that, when applied to a skin friction pattern where saddle points and nodal points occur, topological considerations uniquely define the separation line as one of the two separatrixes passing through the saddle point. A vortex core is associated with the roll up of a stream surface which intersects the body at the separation line, and if this core extends to the surface, its location on the surface is topologically defined by a spiral node.

Topology has been of little use in settling the question as to the nature of crossflow separation. Since there are no saddle points associated with this separation, the separation line cannot be defined as a separatrix. Instead, it is generally defined as the convergence line, the line upon which other skin friction lines converge. There is no agreement as to the nature of this convergence line. Wang claimed that it need not be a skin friction line and may begin anywhere upon the body. Tobak and Peake stated that the separation line is the extension of a skin friction line that began at the node of attachment.

One reason for this lack of agreement is that no one has been able to give a precise definition of the convergence line. It is not uniquely determined by simply defining it as the line upon which other lines converge. All limiting streamlines which are converging upon the convergence line are also converging upon each other, and any one of them can qualify as a convergence line. Therefore, the separation line cannot be precisely determined by the definition of the convergence line.

An attempt at a precise mathematical definiton of the separation line was made by Zhang.[7] He attempted to determine the separation line location by studying the stream surfaces which intersected the body along limiting streamlines. His analysis was flawed by the non-unique definition of his stream surfaces. An infinite number of stream surfaces intersect the body along any given limiting streamline, and these stream surfaces intersect the body at an infinite number of angles.

Although the location of a line upon which the limiting streamlines converge has not been mathematically defined, it can be determined visually from computed limiting streamline patterns or oil flows.

In the limiting streamline pattern, the lines appear to approach one particular line which, in this study, will be called the convergence line. The limiting streamlines seem to become tangent to the convergence line. This would suggest that the convergence line is an envelope, though this has not been proven conclusively in the literature. The character of this convergence line will be examined in Chapter IV.

Even though visual inspection of the limiting streamline pattern will give the convergence line location, it will not determine where separation begins. Separation may begin before or after an apparent convergence line appears. This too will be discussed in Chapter IV.

Since the issues concerning crossflow separation cannot be settled using topological interpretations of limiting streamline patterns, other tools of investigation must be used. Experimental and computational work has done little to answer questions concerning crossflow separation. Oil flow experiments have been used extensively to locate separation on various wings and bodies. However, these experiments give only the limiting streamline patterns and do not provide information about the three-dimensional behavior of the flow. Furthermore, the resolution is not particularly good. In regions where the flow has separated, the viscous forces are often small, the oil pools and does not follow the skin friction lines, and gravity may become a dominant factor. The pooling of oil may also be a problem near the separation line.

The pressure distribution is another flow parameter that is often obtained experimentally, but it cannot be used to determine precisely where separation occurs. The behavior of the pressure distribution near crossflow separation will be discussed in Chapter IV.

The behavior of the three-dimensional flow has been largely determined by various flow visualization techniques. The direction of the flow can be determined by placing tracer particles in the flow, or by allowing dye to wash off a model. Yet these methods are strictly qualitative and do not give enough detail near the onset of crossflow separation to resolve the questions concerning crossflow separation.

Recently, laser interferometry has been introduced into the study of fluid flows. This technique can be used to map the entire three-dimensional velocity field. However, it requires the storage and manipulation of large amounts of data and has not been used to study separation on a fine scale.

Since the experimental and topological approaches do not provide enough information to answer the questions concerning crossflow separation, computational experiments appear to be an attractive means for investigating crossflow separation. Although existing codes have been used primarily for pressure and force calculations, their formulation does not rule out their use for fine scale investigation of other flow parameters such as the velocity fields and vorticity distributions. Three-dimensional thin-layer codes are being used to investigate separation with saddle points on the nose of a hemisphere cylinder,[8] and two-dimensional viscous codes have been used by Wang[1] and Ta Phuoc Loc[9] to study separation from impulsively started cylinders. By using the impulsive flow analogy, comparisons can be made between the separation on an impulsively started cylinder and crossflow separation on a body at an angle of attack. However, there are fundamental differences in the two techniques. For the impulsively started cylinder, the location of separation is well defined by a zero in the skin friction. For crossflow separation on a three-dimensional body, there are no zeroes in the skin friction and the separation location is difficult to define.

In this work a computational code was used to investigate in fine detail crossflow separation on a simple body of revolution, namely, a three-caliber tangent ogive. For a simple body of revolution, crossflow separation can occur with no reverse flow in the axial direction. Therefore, by assuming a supersonic flow, it was possible to utilize a marching code, the parabolized Navier-Stokes code, to study crossflow separation. Computational data were obtained for Mach 2.0 flow at the angles of attack $\alpha = 10°$ and $\alpha = 15°$. For the $\alpha = 10°$ cases, the freestream Reynolds numbers were 12,000 and 300,000. For $\alpha = 15°$, the freestream Reynolds numbers were 12,000 and 150,000. All four cases showed evidence of crossflow separation, and the behavior of the velocity field, the vorticity, pressure, and skin friction were examined near the convergence line.

CHAPTER II
TOPOLOGY AND SEPARATED FLOWS

Topological ideas have proved to be invaluable in the interpretation of continuous vector fields that are defined upon surfaces. In the study of fluids, the vector fields which are commonly interpreted with the aid of topological notions are the skin friction and vorticity fields on the surface of a body and the two-dimensional projections of the velocity fields onto planes. The following is a review of some of the basic topological notions. More extensive treatments of these ideas can be found in references by Tobak and Peake,[3] Flegg,[10] and Legendre.[11]

On the surface of a body, a continuous vector field can be represented by $(u(x,y),v(x,y))$. Lines, $C(x,y) = 0$, are defined so that, at every point on the surface, their direction is given by the value of the vector field at that point,

$$\frac{dx}{u} = \frac{dy}{v} \tag{1}$$

The slope of any line which passes through the point (x,y) is given by

$$\frac{dy}{dx} = \frac{v}{u} \tag{2}$$

If $u \neq 0$, the slope of the line through the point (x,y) is uniquely defined. If $u = 0$ and $v \neq 0$, (dy/dx) is not defined. However, the direction of the line is uniquely defined; it is parallel to the y-axis.

If both $u = 0$ and $v = 0$ at (x,y), the direction of the line or lines passing through (x,y) is not defined, and the point (x,y) is called a critical point. Critical points may be isolated (i.e., no other critical points lie within an arbitrarily small distance of the critical point), they may occur in a line of critical points called a critical line, or they may occur in a region of critical points.

Although many types of critical points may occur in an arbitrary continuous vector field, topological discussions are usually limited to simple critical points. A critical point is a simple critical point if it is an isolated critical point, and if the first order terms in the Taylor series expansions of u and v about the critical point (x,y) are nonzero and linearly independent. If the coordinate system is chosen so that the singular point occurs at the origin, then the first order Taylor series expansions give

$$\begin{aligned} u &= ax + by \\ v &= cx + dy \end{aligned} \tag{3}$$

The equation for the line or lines passing through the critical point is given by

$$\frac{dy}{dx} = \frac{cx + dy}{ax + by} \tag{4}$$

If t is chosen to be a parameter, such as arc length, the above differential equation can be separated into two coupled differential equations,

$$\frac{dy}{dt} = cx + dy$$

$$\frac{dx}{dt} = ax + by \tag{5}$$

If a solution of the form $(x,y) = (A,B)e^{\lambda t}$ is assumed, these coupled differential equations can be rewritten as two linear equations which are then solved for λ and A or B. There are two unique solutions,

$$(x_1,y_1) = (b,\ \lambda_1 - a)A_1e^{\lambda_1 t}$$

$$(x_2,y_2) = (b,\ \lambda_2 - a)A_2e^{\lambda_2 t} \tag{6}$$

where A_1 and A_2 are arbitrary constants and

$$\lambda_1 = \frac{a+d}{2} + \sqrt{\frac{(a+d)^2}{4} - (ad - bc)}$$

$$\lambda_2 = \frac{a+d}{2} - \sqrt{\frac{(a+d)^2}{4} - (ad - bc)} \tag{7}$$

Any linear combination of (x_1, y_1) and (x_2, y_2) will also satisfy equation 4.

Depending upon the values of λ_1 and λ_2, three different types of behavior may occur at a simple critical point (Figure 1). If λ_1 and λ_2 are both real and have opposite signs, the critical point is a saddle point. Only two lines pass through a saddle point, and these lines are called separatrixes. The direction of the vector field is toward the critical point along one separatrix, and away from the critical point along the other. All other lines avoid the saddle point.

If λ_1 and λ_2 are both real and of the same sign, the critical point is a nodal point, and an infinite number of lines share the critical point. The direction of the vector field is away from the node if λ_1 and λ_2 are greater than 0, towards the node if λ_1 and λ_2 are less than 0. For skin friction lines the former is called a node of attachment, the latter a node of separation.

If λ_1 and λ_2 are complex conjugates of each other, the critical point is a spiral node. Again, an infinite number of lines share the critical point. The direction of the vector field is dependent upon the sign of the real part of λ_1 and λ_2. The direction is away from the critical point if the real part is positive, into the critical part if it is negative.

The lines defined by equation 1, the saddle points, nodes, spiral nodes, and other types of critical points make up the phase portrait of the vector field. Generally, only simple critical points occur in skin friction and surface vorticity phase portraits. Nonsimple isolated critical points and critical lines are topologically unstable, and small perturbations in the flow parameters cause these nonsimple critical points and critical lines to be replaced by collections of saddle points and nodes. Small perturbations in the flow conditions will also break connections between two saddle points.

When a topologically stable phase portrait is constructed from a continuous vector field, the number of nodal points and saddle points must satisfy certain topological rules. For any simple closed surface, the number of nodes must exceed the number of saddle points by 2,

$$\Sigma N - \Sigma S = 2 \tag{8}$$

Here, ΣN is the number of nodes and spiral nodes, ΣS is the number of saddle points.

These phase portraits are particularly useful for the study of separated flows in which saddle points occur. In the skin friction pattern of one type of separation on a body of revolution (Figure 2), there is a node of attachment at the nose and there is a node of separation at the rear of the body. On each side of the body there are also a saddle point and a spiral node, and one of the separatrixes that passes through the saddle point winds up into the spiral node. This type of separation has been called the Werle-type separation, since the only known experimental example of this particular combination of a saddle point and spiral node was obtained by Werle.[12]

For Werle-type separation, the saddle point is a saddle point of separation, and the separation line is one of the separatrixes that pass through the saddle. The stream surface that intersects the body at the separation line rolls up about a vortex core which intersects the body at the spiral node. Note that in this interpretation of the flow separation, the number of nodes and saddles satisfy the above rule.

A second type of separation with a saddle point, the horseshoe-type separation, is illustrated for a body of revolution in Figure 3. As in the previous example, there is a node of attachment at the nose and there is a node of separation at the rear. In addition to these two nodes, there are a saddle point and a node of reattachment on the leeward side of the body. The separation line is one of the separatrixes that passes through the saddle. The vortex core does not extend to the surface of the body. It is always off the body and is defined by the roll up of a stream surface which intersects the body at the separation line. Note that this example also satisfies the rule relating the number of nodes and saddles.

The above examples do not exhaust the possibilities for separated flows that have saddle points in the phase portrait of the skin friction lines. However, they are representative of the types of behavior that do occur. For crossflow separation, the skin friction pattern has only lines connecting the nodal point of attachment at the nose with the nodal point of separation at the rear (Figure 4). This is identical to the pattern for attached flow, and the location of the separation cannot be determined by topological means.

In the crossflow planes, crossflow separation exhibits the characteristics of two-dimensional separated flow. By projecting three-dimensional vector fields onto two-dimensional surfaces, such as the velocity field onto the crossflow plane, topological ideas can be used to aid in the interpretation of this type of flow separation.

For two-dimensional surfaces upon which three-dimensional vectors have been projected, the restrictions concerning the types of critical points are less limiting. Depending upon the shape of the surface and/or symmetries in the flow, critical lines may occur. Since small perturbations to the flow field act upon the full three-dimensional vector field, these critical lines do not necessarily disappear, though they may move. Also, saddle-to-saddle connections are allowed. Such connections need not disappear when small perturbations are made to the three-dimensional flow field.

The most common two-dimensional projection of a three-dimensional vector field used in the study of separated flows is the projection of the velocity field onto a plane. For a body of revolution, this plane is usually chosen to be the crossflow plane. Due to the no-slip boundary condition for viscous flows, a critical line always occurs at the surface of a stationary body. To avoid treating the surface as a critical line, a direction is defined at the surface by

$$\frac{dy}{dx} = \lim_{z \to 0} \left(\frac{\partial v}{\partial z} \Big/ \frac{\partial u}{\partial z} \right) \tag{9}$$

where z is the normal to the surface. This in effect defines (dy/dx) at the surface of the body to be the direction of the flow a small distance off the body. Since directions are now assigned to the points on the surface, the critical line at the surface is replaced by a non-critical line and simple critical points. These simple critical points are called half nodes and half saddles.

Generally, in these crossflow planes, there are no critical lines or nonsimple critical points. The rule relating the number of simple critical points in a crossflow plane that cuts through a simply connected three-dimensional body is

$$\Sigma N + 1/2\,\Sigma N' - \Sigma S - 1/2\,\Sigma S' = -1 \tag{10}$$

where ΣN is the number of nodes, $\Sigma N'$ is the number of half nodes, ΣS is the number of saddle points, and $\Sigma S'$ is the number of half saddles.

An example of a crossflow phase portrait for separated flow is shown in Figure 5. In this example there are both primary and secondary separations. There are four spiral nodes in the flow, a saddle point off the leeward side of the body, and eight half saddles. The use of topology in constructing this crossflow velocity pattern indicates the direction of the roll up for the secondary separation.

Care must be taken when applying the topological notions reviewed above to crossflow planes. Since the velocity field is only a two-dimensional projection, discrepancies can occur in the interpretation of the flow. The angle of the plane cutting through the body affects the location of the half saddles which are associated with the separation and the location of the spiral nodes. It can even cause the behavior of the spiral node to change. A change in the angle of the plane can cause the lines to spiral away from instead of into the node.[6]

The use of the crossflow plane can also lead to a false identification of flow separation. For instance, when a negative crossflow first occurs on a tangent ogive, the crossflow velocity field indicates an apparent reverse flow in the boundary layer. It can also indicate a rotation of the fluid about a central core which lies outside the boundary layer. The natural interpretation of this crossflow behavior would be that separation has occurred and a vortex exists in the three-dimensional flow. However, when the three-dimensional flow is examined, there are no indications of vortices or separation. The flow squeezes together and the boundary layer thickens, but not at a rate which introduces new structures into the flow. The full three-dimensional character of the flow must be kept in mind when crossflow planes are interpreted.

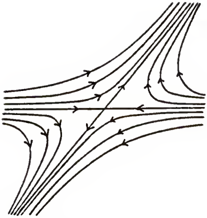

SADDLE POINT

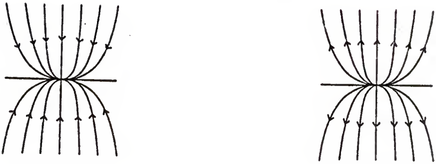

NODE OF
SEPARATION

NODE OF
ATTACHMENT

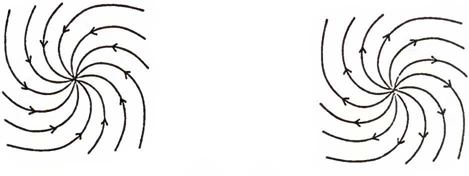

SPIRAL NODES

Figure 1. Simple critical points.

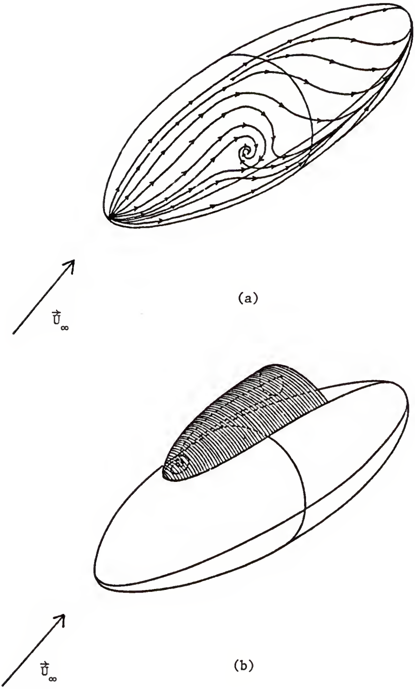

Figure 2. Werle-type separation. a) Limiting streamline pattern; b) Surface of separation. The view in (b) is rotated 90° from the view in (a).

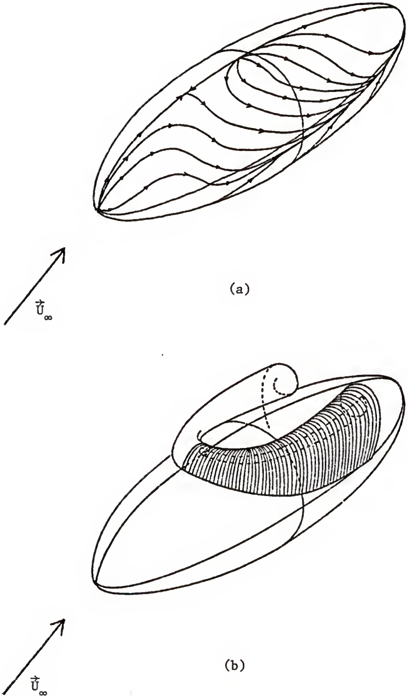

Figure 3. Horseshoe-type separation. a) Limiting streamline pattern; b) Surface of separation.

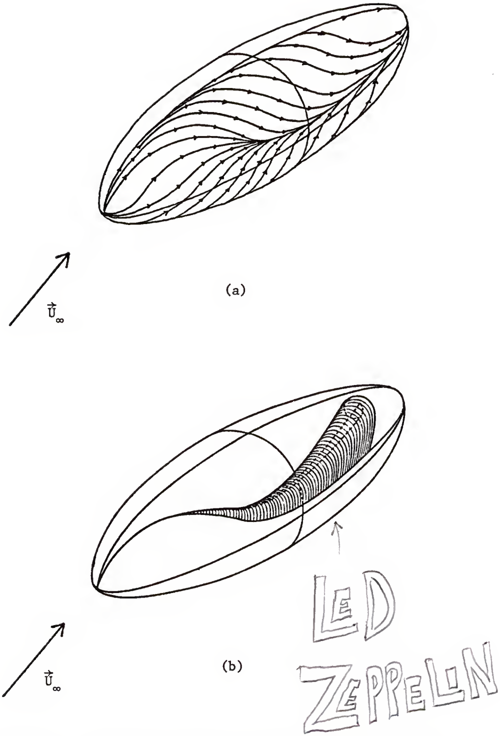

Figure 4. Crossflow separation. a) Limiting streamline pattern; b) Surface of separation.

LED ZEPPELIN

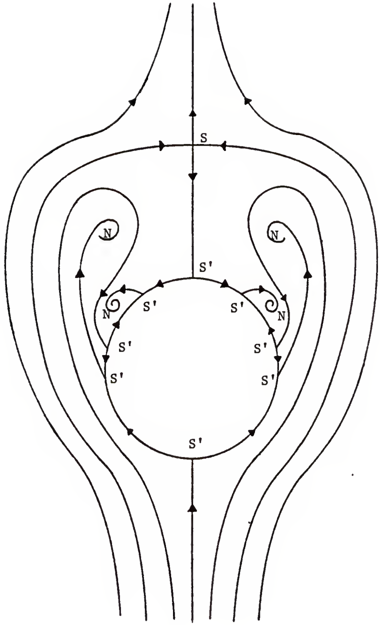

Figure 5. Primary and secondary separations for a body of revolution. In this crossflow velocity pattern, there are four nodes, one saddle, and eight half saddles.

CHAPTER III
PARABOLIZED NAVIER-STOKES CODE

Background

The parabolized Navier-Stokes (PNS) codes were developed as efficient methods of computing three-dimensional, steady, supersonic, viscous flows. The efficiency of these codes was achieved by treating the governing equations, the PNS equations, as an initial value problem, thus allowing the utilization of a space-marching finite-difference technique. The PNS codes solve the governing equations in a series of computational planes. At any given computational plane, the flow in the upstream planes has already been calculated and upstream information is available for calculating the flow at the computational plane. No downstream information is available. This limits the types of problems which can be solved using the PNS codes to those in which the upstream traveling influences are small.

Several assumptions concerning the nature of the governing equations must be made if the solutions are to be marched down the body. The viscous terms which contain partial derivatives with respect to the streamwise direction must be assumed to be negligible and dropped from the equations. This assumption is usually justified for Reynolds numbers much larger than one[13] and is inherent in the thin-layer approximation of the Navier-Stokes equations customarily used as a starting point for the derivation of the PNS equations. The thin-layer approximation is not necessary for the stability of the PNS space-marching scheme, but it appears to be a reasonable one. Two-dimensional tests for Reynolds numbers greater than 10,000 have shown that the thin-layer approximation does not affect the accuracy to the fourth significant digit.[13]

The space-marching characteristic of the PNS code places other restrictions on the flow behavior. Since no downstream information is available, there can be no reverse flow in the streamwise direction, and the flow must be supersonic. For viscous flows, this last condition is always violated near the surface of the body. In the subsonic region of the boundary layer, downstream information does propagate upstream. The inability of the PNS code to treat these upstream traveling influences can lead to instabilities in the solution procedure unless the pressure terms in the boundary layer receive special treatment. For tangent ogive computations, the treatment of these pressure terms reduces to setting the static pressure derivative, $\partial p/\partial r$, equal to 0 in the subsonic region of the boundary layer. The variable r lies in the computational plane and is normal to the body in the computational plane.

The PNS code which was adapted for this investigation of crossflow separation is based on the Schiff-Steger equations[14] and was developed by Rai and Chaussee.[15] Its finite differencing scheme is second order accurate in the marching direction and fourth order accurate in the crossflow direction. It uses an implicit method to solve the PNS equations in the computational plane. The initial data for the solutions were determined using the PNS code in the stepback mode. The available turbulence model was not used. Questions concerning the validity of turbulence models would further complicate the discussion of crossflow separation.

Gridding

The solutions of Navier-Stokes codes are highly dependent upon the gridding technique used. A large circumferential grid spacing in areas of rapid changes can smooth out jumps or can cause oscillations and instabilities in the solutions. The location of the first grid point off the surface also plays an important role in the stability and the resolution of the solutions. Several changes were made to the gridding scheme of the PNS code to minimize high order oscillations in the solutions and to improve the resolution of the solutions at separation.

In the PNS code, the outer boundary of the grid in the computational plane is coincident with the bow shock. The bow shock is assumed to be a sharp discontinuity, and its location is determined from shock fitting procedures and information from previously computed planes.[13] Since the bow shock is assumed to be a sharp discontinuity, no grid clustering at the bow shock is necessary, and the majority of the grid points can be clustered near the surface of the body where the mechanisms driving the separation are located.

In the unadapted code, the grid points all lie along lines which radiate from a point located inside the body surface. For bodies of revolution, this point is taken to be where the longitudinal axis of the body intersects the computational plane. A designated percentage of the points along these radial lines can be algebraically clustered toward the surface by one of two methods. The first gives the distance between adjacent grid points on the kth radial line as

$$ds(k,l+1) = (1 + \varepsilon \cdot ss)ds(k,l) \tag{11}$$

Here, ε and ss are constants which insure that the last point lies on the bow shock. The distance of the first point off the surface, ds(k,1), has the same value for all radial lines in the computational plane. The second method uses the same clustering equation, but the ratio, ds(k,1)/d(k), is kept constant. Here, d(k) is the distance from the surface to the shock along the kth radial line.

The choice of ds(k,1) or ds(k,1)/d(k) does not vary as the solution is marched down the body. This leads to difficulties in obtaining solutions with good resolution in the boundary layer. For instance, when the second clustering method was used on the nose of a three-caliber tangent ogive, the value of ds(k,1)/d(k) would be adjusted so that the velocities of the flow at the first grid points off the surface were within the suggested range of 0.1 to 0.15 times the free stream velocities in the initial computational plane. In a computational plane a body diameter down the ogive, the velocities at the first grid points off the surface were 0.2 to 0.3 times the freestream velocity. To maintain good boundary layer resolution, the value of ds(k,1)/ds(k) was halved, and the PNS code was restarted using the restart option. Although the restart option automatically interpolates the flow solution onto the new grid, large errors were introduced into the solution. Some of the manifestations of these errors were high order oscillations in the skin friction direction. These oscillations eventually would damp out, but then a new change in the value of ds(k,1)/ds(k) was required, and new oscillations were introduced. Careful examination of crossflow separation was not possible with this gridding scheme.

An additional problem in the choice of a constant ds(k,1) or ds(k,1)/d(k) is the circumferential change in the boundary layer thickness which occurs with crossflow separation. When the value of ds(k,1)/ds(k) was chosen so that the velocity criteria were met on the windward side of the separation, the velocities at the first grid points off the surface on the leeward side of the separation were much too small, and the solution would not march. Conversely, if ds(k,1)/d(k) was matched to the velocities on the leeward side of the separation, the resolution on the windward side was not good.

In the code adapted for this investigation, ds was varied from plane to plane and from radial line to radial line according to

$$ds(i+1,k,1) = ds(i,k,1) \cdot const/Mach(i,k,1) \qquad (12)$$

where i denotes the computational plane and k the radial line. The constant was chosen to be 0.2 so that the suggested velocity criteria would be met for Mach 2 flow. To maintain reasonable smoothness and orthogonality in the grid, ds(i,k,1) was approximated by a finite Fourier cosine series,

$$\begin{aligned} ds(i,k,1) = a_o(i) + a_1(i)\cos\big(\phi(k)\big) + a_2(i)\cos\big(2\phi(k)\big) \\ + a_3(i)\cos\big(3\phi(k)\big) \end{aligned} \qquad (13)$$

In this expression, $\phi(k)$ is the angle of the kth radial line measured from the windward side. A cosine series was chosen because of the symmetry across the $\phi = 0°$ line.

When the values of the a_m were allowed to change without bound, they would over-correct the grid and cause oscillations in the leeward and windward pressure distributions or cause the solution procedure to stop. As a result, limitations were placed upon the changes in a_m as follows:

$$(a_m(i+1) - a_m(i))/a_m(i) < \varepsilon \qquad m = 0,1,2,3 \qquad (14)$$

or

$$a_m(i+1)/a_o(i+1) < \delta \qquad m = 1,2,3 \qquad (15)$$

The values of ε and δ were changed after the solution had marched the distance of a body diameter. The changes in the a_m's from one plane to the next were at most a few percent. Hence, the grid changed gradually and smoothly from one plane to the next, and respacing of the solutions in the previous computational planes was not necessary.

In all the computations, the number of grid points along the radial lines was chosen to be 45. The percentage of these points which were algebraically clustered toward the surface of the body was chosen to be 95%.

Oscillations were also introduced into the leeward and windward pressure distributions when changes in the axial step size were made. In order to minimize the effects of changing step size, the step size was chosen to be 0.05 inch from 0.04 to 0.57 calibers aft of the nose and then kept at a constant 0.1 inch for the remaining length of the body.

The above adaptations to the gridding procedure reduced the high order oscillations in the skin friction direction and improved the resolution of the boundary layer. To improve the resolution of the solutions near separation, the radial lines were clustered circumferentially with a cubic clustering function. In all the computations, the number of radial lines was chosen to be 73. The largest spacing occurred at the windward side of the ogive where the angular spacing between the first and second radial lines was 5°. For $\alpha = 10°$ and Re = 300,000, the spacing on the leeward side was 3°. The minimum spacing of 1.6° occurred 60° from the leeward side. This gave good resolution in the region where the skin friction lines first began to converge onto a line. For the other computations, the spacing at the leeward side was 4°, and the minimum spacing of 1.2° occurred 80° from the leeward side. This choice of clustering gave good resolution near the convergence line. The circumferential clustering was kept constant for the length of the body for the $\alpha = 10°$ computations. For $\alpha = 15°$, the solution initially would not march with clustering in the circumferential direction. The solution was marched from 0.04 to 0.57 calibers aft of the nose with no clustering. At 0.57 calibers, the grid was clustered, the stored solution was respaced, and the solution was marched down the body.

The clustering of the grids in the circumferential direction did not appreciably affect the solutions before the skin friction lines began to converge strongly. After the skin friction lines began to converge strongly, the clustering stabilized the behavior of the skin friction near the convergence line.

Smoothing Coefficients

In the PNS code, implicit and explicit damping terms are added to damp out higher order oscillations.[13] The explicit damping term is a fourth order term and involves two parameters, SMU and EPSB. SMU is the primary mechanism for controlling the size of the explicit term. An implicit damping term is also added and is sized by SMUIMP. A fourth term, EPSA, is added so that the primary diagonal of the block tridiagonal matrix which is inverted in the solution procedure never goes to zero and insures that the block tridiagonal matrix is invertible. It can add sources and sinks to the flow if it is allowed to become too large.

The effect of the four terms on the leeward and windward pressures and on the error in the mass flux was examined for $\alpha = 10°$ and Re = 300,000. It was determined that SMU and SMUIMP had little effect on the high order oscillations in the windward and leeward pressure distributions and on the mass flux error. Their values were chosen to be 0.4 and 1.2 respectively.

The parameters EPSA and EPSB were chosen to be equal. For EPSA and EPSB equal to 0.4, oscillations occurred in the windward and leeward pressure distributions. These disappeared for EPSA = EPSB = 0.1. The mass flux error was reduced to less than 0.1% when the smaller values of EPSA and EPSB were used.

For the $\alpha = 10°$, Re = 12,000 computation, the smoothing parameters were left at the values indicated above. For $\alpha = 15°$, oscillations in the leeward and windward pressures became undesirably large. These were smoothed out by choosing a slightly larger value of EPSA and EPSB, namely, 0.2. For $\alpha = 15°$, the mass flux errors were typically around 1%.

CHAPTER IV
RESULTS AND DISCUSSION

Comparison of Computational to Experimental Behavior

A three-caliber tangent ogive was used for all the computations of crossflow separation. The diameter of the cylindrical portion of the ogive was 3.0 inches. The freestream Mach number was kept at 2.0, and the freestream temperature was fixed at 290° Rankine. The wall temperature was chosen to be constant and was fixed at 500° Rankine. In the PNS code, the viscosity coefficient is calculated by Sutherland's formula and is a function of the temperature only. Since the temperature at the surface of the body was chosen to be constant, the viscosity coefficient was also constant at the surface.

Computational data were obtained for $\alpha = 10°$ and $\alpha = 15°$. For $\alpha = 10°$, the free stream Reynolds numbers were chosen to be 12,000 and 300,000. For $\alpha = 15°$, the free stream Reynolds numbers were 12,000 and 150,000. The solutions were marched down the ogive until the crossflow separation was well established.

For Mach number = 1.98, $\alpha = 15°$, and Re = 150,000, the values of the static pressure coefficients at the surface of the tangent ogive were computed by the PNS code and were compared to experimental data obtained by Jorgensen and Perkins.[16] The results of this comparison are shown in Figure 6 for 2.0, 3.0, and 5.0 calibers aft of the nose. At 2.0 calibers aft of the nose, the curve of the computed static pressure coefficient is shifted above the experimental curve. This discrepancy may have been caused by errors in the starting solution or by experimental errors. At 3.0 calibers aft of the nose, the computational pressure distribution is again shifted above the experimental distribution on the windward side, but the amount of the shift is less than that at 2.0 calibers. At 5.0 calibers, the two distributions show excellent agreement on the windward side. This behavior indicates that the cause of the disagreement in the computational and experimental pressure curves became less important as the distance from the nose increased.

In Figure 6, the computed static pressure distribution is either shifted a constant amount above or coincides with the experimental distribution on the windward side. This is not the case on the leeward side at 3.0 and 5.0 calibers aft of the nose. This behavior can be explained by the presence of turbulence effects in the experimental data. For Re = 150,000, the flow should be laminar on the windward side and the experimental pressure distribution should agree with those determined from laminar computations. As discussed above, at 2.0, 3.0, and 5.0 calibers aft of the nose, the only difference in the computational and experimental pressure distributions on the windward side is a constant. On the other hand, for Re = 150,000, the flow separation should become turbulent somewhere on the ogive, and hence the experimental pressure gradients on the leeward side should show some effects of the turbulent separation. Since the computations were forced to be laminar, the computational and experimental pressure gradients cannot be expected to agree, and they do not agree at 3.0 and 5.0 calibers aft of the nose. The disagreement in the two windward pressure distributions can therefore be explained by the absence of turbulence effects in the computational data and by their presence in the experimental data.

A further check on the behavior of the PNS code was made by comparing the behavior of the limiting streamlines for different Reynolds numbers and angles of attack. These limiting streamlines were not calculated by using the flow direction, u/v, at the first point off the surface, as is commonly done in computational fluid dynamics. Instead, the directions of the limiting streamlines were determined by taking the limit of u/v as the normal distance to the surface approached 0. This procedure took into account the skewing of the velocity field that takes place near the surface.

In Figures 7 and 8 the limiting streamline patterns for a constant angle of attack, $\alpha = 10°$, and two Reynolds numbers, Re = 300,000 and Re = 12,000 are shown. In these limiting streamline patterns, the convergence line appears closer to the nose for Re = 300,000 than for Re = 12,000. In both cases, the convergence line approaches a constant value of ϕ as the distance from the nose is increased. For Re = 300,000, this constant value is approximately 70°; for Re = 12,000, this value is 90°. The dependency of the location of the convergence line upon the Reynolds number agrees with experimental evidence that indicates that laminar flow separation occurs closer to the nose for higher Reynolds numbers and that, on a yawed cylinder, flow separation occurs more toward the windward side for higher Reynolds numbers.

In Figure 7 there is evidence of a strong secondary separation for Re = 300,000. Due to rapid changes in the solution near the secondary separation, the gradients were large and the solution was not stable in this region. The direction of the limiting streamlines near the secondary separation oscillated as the solution was marched. Eventually, these oscillations forced the marching procedure to stop. The effect of these oscillations can be seen in the limiting streamline pattern in Figure 7. As the distance down the body increases, the limiting streamlines at first converge upon one well defined line and then begin to diverge.

In Figures 8 and 9 the limiting streamline patterns for a constant Reynolds number, Re = 12,000, and two angles of attack, $\alpha = 10°$ and $\alpha = 15°$, are shown. In these patterns the limiting streamlines converge more rapidly onto a convergence line for $\alpha = 15°$ than for $\alpha = 10°$. This behavior agrees with experimental evidence that indicates that separation occurs nearer the nose for larger angles of attack. For both $\alpha = 10°$ and $\alpha = 15°$, the convergence line approaches a constant value of 90°. Subsonic studies in the University of Florida tow tank at Re = 12,000 indicated a small difference in these two values, but both experimental values were close to 90°.[17]

The solutions computed by the PNS code agree well with available pressure data and show the proper dependency of the separation location upon the Reynolds number and angle of attack. The usage of the PNS code for study of crossflow separation appears to be justified.

Streamtubes

Representative crossflow velocity fields are plotted in Figures 10 and 11. Note that in Figure 11 the crossflow velocity field seems to indicate that separation and vortical flow have occurred at 2.97 calibers aft of the nose for $\alpha = 15°$ and Re = 12,000. This would be an erroneous interpretation. The appearance of vortical type structures in Figure 11 is due to the squeezing together of the streamlines near the surface. This squeezing induces reverse flow in the crossflow plane.

However, the squeezing is not at a fast enough rate to force the flow away from the body. These crossflow velocity fields cannot be expected to provide a good measure as to when separation begins.

The onset of separation is more accurately determined by examining the behavior of a streamtube which encircles the body. This streamtube is defined as follows. Initially, a circle in a crossflow plane is defined by $r = r_o$ and $x = x_o$ where r is the distance in the crossflow plane from the axis of the ogive and x is the axial distance from the nose. The value of x_o is chosen small enough so that no reverse flow occurs in the crossflow plane at $x = x_o$ and no indications of flow separation are observed for $x < x_o$. The streamtube is then defined by the streamlines which pass through each point on this circle. For computational purposes 360 equally spaced points were used to define the circle. Representative crossflow cuts of these streamtubes are shown in Figures 12-14.

Initially, the squeezing together of the limiting streamlines forces the flow off the surface and a bump occurs in the streamtube. The circumferential location of this bump coincides with the location of the converging streamlines. As the distance from the nose increases, the streamlines continue to converge and the bump in the streamtube becomes a fold. This fold appears before a convergence line can be determined from the limiting streamline pattern. The fold then elongates and moves away from the surface, and the streamlines which were initially chosen to define the surface are clustered onto the fold. A knob, which coincides with a decrease in the Mach number, develops at the end of the fold, and, finally, the fold begins to roll up.

Several values of x_o and r_o were tried, and the behavior of the streamtube was not appreciably affected by changes in x_o and r_o as long as the streamtube stayed well within the boundary layer before separation began. The distance from the nose where the first fold in the streamtube occurred did not change noticeably with changes in x_o and r_o. Therefore, the onset of separation might be defined by the appearance of a fold in the streamtube. This definition implies that separation begins before a convergence line can be determined from visual inspection of the limiting streamlines. This implication is reasonable, since the fold in the streamtube had lengthened considerably and the flow had moved well off the surface before a convergence line could be seen in the limiting streamline pattern.

In Figures 12-14, the folds in the streamtubes widen considerably near the ogive's surface. This widening occurred even when the initial circle was very close to the surface of the ogive and was between the surface and the first grid points off the surface. This seems to indicate that the squeezing of the fluid off the surface occurs in an extended region and not just in the immediate area of one line, as would be the case if the fold remained narrow all the way to the ogive's surface. Because of this widening, the streamtubes seem to be leaving the surface tangentially in Figures 12b, 12c, 13b, 13c, 14b, 14c, and 14d. This tangential character of the flow separation will be discussed later in this chapter.

When a definite fold occurs in the streamtube, a line can be extrapolated from the center of the fold to the surface of the body. In Figure 14c, it appears that such a line could possibly intersect the surface at the convergence line, but the widening of the fold at the ogive's surface makes it impossible to determine exactly where and how this line intersects the body's surface. The resolution of the computed data was not sufficient to warrant a limiting procedure to determine the existence of a limit line through the center of the fold, and if such a line existed, where and how it intersected the surface.

The results from this streamtube technique imitate those obtained by Intemann in the University of Florida tow tank.[17] In his experiments, a model was painted with dye, and, as it was towed through the tank, the dye washed off the model and defined a streamtube. The use of a light plane made it possible to study crossflow cuts of this streamtube. The computed results shown in Figures 12-14 were in excellent agreement with those obtained by Intemann. His results indicated that, during separation, a fold first occurred in the streamtube. This fold then elongated and eventually rolled up. His results also indicated that the streamtube appeared to be leaving the model's surface tangentially.

Crossflow Information

In Figures 15-22 the Mach number, pitot pressure, static pressure, and vorticity distributions are shown for various crossflow locations. The plotted distributions were taken from the $\alpha = 10°$ and $Re = 300,000$ computation and the $\alpha = 15°$ and $Re = 12,000$ computation.

At 2.97 calibers aft of the nose, the Mach number plots show that there is a thickening in the boundary layer on the leeward side. This thickening is represented in the plots by an increase in the thickness of the shaded areas. The boundary layer is thickest in a region which corresponds to the bump in the streamtube. When the fold in the streamtube has developed and begun to elongate, Figure 15 shows an increase in the boundary layer thickness in the region of converging streamlines and a decrease in the thickness of the boundary layer at the leeward side. For the high Reynolds number case, the lengthening and rolling up of the fold in the streamtube correspond to the appearance of a sheet and core of lower Mach number flow. At the vortex core, the flow in the axial direction is retarded with respect to the surrounding flow. This behavior also occurs for the low Reynolds number case, but it is a weaker effect and cannot be seen with the scaling of the shades used in these plots.

Figures 17 and 18 show the pitot pressure for the two cases. Since the pitot pressure is a function of the Mach number, there is a great deal of similarity between the Mach number and pitot pressure plots. At 2.97 calibers aft of the nose, the low pressure areas extend slightly farther into the flow in the region of converging streamlines, but no separation is indicated by the plots. At 3.64 calibers a fold in the streamtube has developed, and both plots show an increase in the thickness of the low pressure regions near the converging streamlines and a decrease in the thickness of the low pressure regions on the leeward side. When the folds in the streamtube have elongated and begun to roll up, the lower pressure areas extend well into the flow just to the leeward side of the convergence line, while the low pressure regions remain close to the body at the leeward side. For the high Reynolds number case, there is an area of low pitot pressure which coincides with the core of the rolled up fold. With the scale of these plots, a core cannot be seen for Re = 12,000; however, investigation of the numerical data indicated that a weak core did exist.

The static pressure plots (Figures 19 and 20) do not yield much information concerning the nature of crossflow separation. They do indicate that the normal pressure gradients are small. This can be seen in the lack of shade change as the radial distance from the body increases. The static pressure in the subsonic region of the boundary layer was forced by the PNS code to be independent of the radial direction. These plots show that the static pressure is also independent of the radial direction in the supersonic boundary layer. This behavior agrees with boundary layer assumptions and indicates that the treatment of the pressure gradient in the boundary layer by the PNS code was reasonable.

In the $\alpha = 10°$, Re = 300,000 plots, a static pressure maximum occurs between the primary and secondary separation. At 4.31 calibers aft of the nose, these plots show a "core" of minimum static pressure which coincides with the location of the streamtube roll up.

In Figures 21 and 22, the behavior of the vorticity magnitude is shown. Before there is any evidence of separation in the streamtube behavior, the plots indicate that, in the radial direction, a vorticity maximum exists off the surface. This maximum is represented by a change of dark to light to dark as the radial distance from the body is increased and can be seen on the leeward side of the vorticity plots at 2.97 calibers aft of the nose. As the distance from the nose is increased, the existence of this maximum becomes more pronounced until a well defined vortex sheet can be seen leaving the surface in what appears to be a tangential manner. The thickness of the vortex sheet near the surface and the resolution of the plots and calculations, however, do not rule out the possibility of a small angle. This tangential behavior will be discussed later.

The vorticity plots indicate that the strong surface vorticity from the windward side of the body is fed into this sheet. The plots show no indication as to the location of the vortex core.

Tangential Separation

In several of the crossflow methods discussed above it appears that the separated flow is leaving the surface tangentially, but the resolution of the experimental and computational data was not adequate to determine if the separation was indeed tangential. An almost continuous set of data near the surface would be necessary to resolve this issue. It should, however, be noted that if a plane cutting through the ogive shows that the separation is tangential, the separation point cannot be a half saddle. The angle, θ, between the two separatrixes that pass through a saddle point is given by

$$\cos(\theta) = \frac{b^2 + (\lambda_1 - a)(\lambda_2 - a)}{\sqrt{(b^2 + (\lambda_1 - a)^2)(b^2 + (\lambda_2 - a)^2)}} \tag{16}$$

where the constants a, b, λ_1, and λ_2 have already been defined in Chapter II. The separatrixes are parallel if $\cos(\theta) = \pm 1$. A manipulation of the above equation indicates that this can happen only when $\lambda_1 = \lambda_2$, and the critical point is a node. Thus, the separation point in the crossflow plane cannot be a half saddle if the separation is tangential.

In the crossflow plane, however, the limitations on the types of critical points that may occur are not as strict. There may be a critical line which approaches the separation point tangentially, or the separation point may be a nonsimple critical point. One example of a nonsimple critical point is illustrated in Figure 23. Because of the three-dimensional nature of the flow, this point need not be unstable. Furthermore, for this example, the continuity equation does not place any unusual restrictions on the component of the velocity normal to the crossflow plane.

Surface Information

In Figures 24-41, the behavior at the surface of the skin friction direction, skin friction magnitude, vorticity, pressure, circumferential pressure gradient, and flow angle are shown. In Figure 24, the regions of reverse crossflow are shown in gray. In all three cases, a large region of flow on the leeward side went from positive crossflow to negative crossflow within the space of two space-marching steps or 0.067 calibers. This change was not caused by rapid changes in the flow direction, as can be seen in Figure 25.

In Figure 25, the skin friction angle, $\arctan(\tau_\phi/\tau_{ax})$, is plotted versus the circumferential angle for $\alpha = 10°$ and Re = 300,000. Here, τ_ϕ is the value of the skin friction in the circumferential direction, and τ_{ax} is the value of the skin friction in the axial direction. At a distance of 2.0 calibers aft of the nose, there is an extended region on the leeward side for which the skin friction angle is small and positive. In this region, there is a small positive crossflow term, but the limiting streamlines are primarily pointing in the axial direction. At 2.31 calibers aft of the nose, there is an extended region on the leeward side for which the skin friction angle is small and negative. There is a small negative crossflow term, but the flow is still primarily in the axial direction. Hence, the initial appearance of reverse flow in the crossflow plane is the result of a small change in the flow direction and does not imply that separation has occurred or is about to occur.

In Figure 24, the location of the convergence line can be determined visually from the limiting streamline pattern at a distance of 1.5 to 2.5 calibers after the initial occurrence of reverse crossflow. Before this point, it is impossible to pick out a single line which becomes the convergence line; instead, it appears that all the skin friction lines are squeezing together to form one line instead of converging upon one specific line. After a convergence line has been established, it appears that the convergence line behaves as an envelope; lines which are started off the convergence line quickly approach the convergence line and merge with it (Figures 7-9).

To determine whether or not the convergence line is an envelope, a function F(n,x) was defined by

$$F(n,x) = \frac{\tau_\phi}{\tau_{ax}} - \left(\frac{\tau_\phi}{\tau_{ax}}\right)_{n=0} \tag{17}$$

In this expression, τ_ϕ is the value of the skin friction in the circumferential direction, τ_{ax} is the value of the skin friction in the axial direction, x is the axial location of a point on the convergence line, and n is the normal distance from the convergence line (Figure 26). If a convergence line could not be defined, $n = 0$ was chosen to be in the center of the bundle of converging lines. In Figure 27, F(n,x) is plotted for several axial locations on the ogive. In these plots, it can be seen that as the axial distance from the nose is increased, the limiting streamlines approach the convergence line more quickly. This is indicated by an increase in the slope, $\partial F/\partial n$, at $n = 0$. In all cases, a maximum value for $(\partial F/\partial n)_{n=0}$ is reached at a finite distance down the body. This maximum occurs after a fold in the streamtube has occurred, and in two of the cases, $\alpha = 10°$, Re = 300,000 and $\alpha = 15°$, Re = 12,000, after the fold has begun to roll up. Once this maximum is reached, $(\partial F/\partial n)_{n=0}$ remains constant or decreases slightly as the distance from nose is increased. Hence, the slope, $\partial F/\partial n$, is finite for all axial locations on the ogive, and the Lipshitz condition is met by the function F(n,x). A unique solution exists for the limiting streamline at n = 0, and, therefore, the convergence line is not an envelope.

In Figure 27, it appears that, when a convergence line can be determined from the limiting streamline pattern, n = 0 is either an inflection point of F(n,x) or very close to an inflection point. This inflection point is caused by the convergence of the limiting streamlines onto a line. For small n, the limiting streamlines are almost parallel to the convergence line, and F(n,x) is small. As the distance from the convergence line increases, the limiting streamlines are converging more rapidly onto the convergence line, and F(n,x) increases. As the distance from the convergence increases further, the limiting streamlines approach the convergence line less rapidly, and F(n,x) begins to decrease. This behavior is shown in Figure 28. Because of this behavior of the limiting streamlines, the function F(n,x) must have an inflection point, and this inflection point appears to lie close to the convergence line for separated flow.

It may be possible to define the separation line as the line where

$$\frac{\partial^2}{\partial n^2}\left(\frac{\tau_\phi}{\tau_{ax}}\right) = 0 \qquad (18)$$

In this expression, n is always normal to the limiting streamlines. This line does not necessarily lie on the convergence line, nor is it necessarily a limiting streamline. It is a mathematically well defined line that lies near the convergence line. As will be discussed later, there is no particular behavior of the three-dimensional flow field which indicates that the separation line should be identified with the convergence line.

The behavior of skin friction magnitude is illustrated in Figures 29-32. As shown in these figures, there are no abrupt changes in the skin friction as the limiting streamlines squeeze together and force the flow off the surface. The minimum skin friction line shown in Figure 31 was defined by $\partial\tau/\partial\phi = 0$ where τ is the magnitude of the skin friction and ϕ is the circumferential angle. In Figure 32 the skin friction magnitude is plotted versus the distance normal to the convergence line. These plots show that once a well defined convergence line exists, the minimum skin friction lies to the leeward side of the convergence line and appears to be a constant distance from the convergence line. This distance is not affected by the presence of a secondary separation for $\alpha = 10°$, Re = 300,000.

This difference in the location of the convergence line and the minimum skin friction line was shown theoretically by Hirschel and Kordulla.[18] A simplified argument follows. Consider a flat surface upon which a convergence line with no curvature exists. The skin friction vector is defined to be (τ_x, τ_y) where the x-axis is aligned with the convergence line, and the y-axis is normal to the convergence line. The skin friction is a minimum when $\sqrt{\tau_x^2 + \tau_y^2}$ is a minimum, or when

$$\tau_x \frac{\partial \tau_x}{\partial y} + \tau_y \frac{\partial \tau_y}{\partial y} = 0 \qquad (19)$$

Expanding τ_x and τ_y in a Taylor series in y and keeping only first order terms in y gives

$$\tau_x\Big|_{y=0} \frac{\partial \tau_x}{\partial y}\Big|_{y=0} + y\left[\left(\frac{\partial \tau_x}{\partial y}\Big|_{y=0}\right)^2 + \left(\frac{\partial \tau_y}{\partial y}\Big|_{y=0}\right)^2\right] = 0 \qquad (20)$$

This first order approximation indicates that the minimum skin friction line is a distance

$$y_{min} = - \frac{\tau_x\Big|_{y=0} \dfrac{\partial \tau_x}{\partial y}\Big|_{y=0}}{\left(\dfrac{\partial \tau_x}{\partial y}\Big|_{y=0}\right)^2 + \left(\dfrac{\partial \tau_y}{\partial y}\Big|_{y=0}\right)^2} \qquad (21)$$

from the convergence line.

The denominator in the above equation is always positive, and so is $\tau_x\big|_{n=0}$ for crossflow separation. If the flow is attached for negative values of y and separated for positive values of y, the flow should slow as y becomes positive. This implies that $\frac{\partial}{\partial y} \sqrt{\tau_x^2 + \tau_y^2} < 0$ or, at $y = 0$, $\partial\tau_x/\partial y < 0$. Therefore, y_{min} is positive, and the minimum skin friction line lies in the separated region of the flow. This result agrees with the computational results.

Since the viscosity coefficient is constant on the surface of the body, the magnitude of the surface vorticity is proportional to the magnitude of the skin friction. The results cited above for the skin friction can also be applied to the vorticity magnitude. In Figure 33 regions where $\frac{\partial|\vec{\omega}|}{\partial r}$ is negative have been plotted in gray; $|\vec{\omega}|$ is the vorticity magnitude, and r is the normal to the surface of the body. The area of negative $\frac{\partial|\vec{\omega}|}{\partial r}$ lies on the windward side of the convergence line and parallels it. It is this region that appears to be feeding the separated vortex sheet in Figure 22.

The behavior of the static pressure distribution on the surface of the ogive is shown in Figures 34-38. The plots of the pressure coefficient distribution give very little information because of the flatness of the distributions; the plots of the pressure gradients in Figures 36 and 37 yield much more information near separation. The pressure gradients indicate that the convergence line lies near and parallel to a minimum and maximum in the pressure coefficient and a maximum in the pressure gradient. The minimum pressure and the maximum pressure gradient occur on the windward side of the convergence line; the maximum pressure on the leeward side.

The minimum skin friction, the minimum and maximum static pressures, and the maximum pressure gradient all lie parallel to but are not coincident with the convergence line. To determine exactly what the flow is doing near the convergence line, the angle U_r/U_t was studied where U_r is the velocity normal to the surface and U_t is the velocity tangent to the surface. From the continuity equation and the boundary conditions, it can be shown that $U_t = f(x,r,\phi)r$ and $U_r = g(x,r,\phi)r^2$. In these expressions, x is the axial distance from the nose, r is the distance from the surface, ϕ is the circumferential angle, and f and g are functions that are finite at $r = 0$. On the surface the ratio U_r/U_t is equal to 0 unless $\partial U_t/\partial r|_{r=0} = 0$. This occurs only at a critical point in the skin friction pattern. For crossflow separation the only critical point in the region of interest is at the nose. Hence, the ratio U_r/U_t is zero everywhere in the region near the convergence line.

The first derivative, $\partial(U_r/U_t)/\partial r$, is nonzero at the surface and is a measure of the flow direction at a small distance off the surface. The computed values of $\partial(U_r/U_t)/\partial r$ are shown in Figures 39-41. Note that the flow appears to be moving off the surface more rapidly on the windward side of the separation line. The line of maximum $\partial(U_r/U_t)/\partial r$ occurs in a region where the normal derivative of the total vorticity is less than 0, and it parallels but does not coincide with the convergence line. There are no abrupt jumps in the plots of $\partial(U_r/U_t)/\partial r$ that might indicate where separation began. Instead, the plots of $\partial(U_r/U_t)/\partial r$ versus n change continuously from a fairly flat profile to one with a pronounced peak on the windward side of the convergence line as the distance from the nose increases and the skin friction lines squeeze together to form a convergence line. This last result was surprising and appeared to contradict Lighthill's argument concerning the squeezing of the flow away from the surface.[19]

Lighthill defined a streamtube which extended from the surface to a small distance off the surface. Using a flux argument, he showed that the height of the streamtube, h, was equal to $\sqrt{\text{const}/(d\tau)}$ where d is the distance between the limiting streamlines and τ is the skin friction magnitude (Figure 42). From the limiting streamline plots (Figures 7-9), it appeared that the squeezing together of the limiting streamlines (change in d) would be the dominating factor near the convergence line, and that the flow should be leaving the surface most rapidly at the convergence line. Furthermore, the decrease in the skin friction as the convergence line is approached from the windward side would only amplify this effect.

However, the maximum value of $\partial(U_r/U_t)/\partial r$ occurs a full 10° on the windward side of the convergence line for the two Re = 12,000 cases, and the flow is not leaving the surface with the largest angle at the convergence line. To study the height change in the streamtubes defined by Lighthill, a parameter, stretch, was defined as follows. The end points, a and b, of an infinitesimally thin streamtube were chosen to lie upon a radial line. The point a lies on the surface, and b is 0.0001 inch off the surface. At 0.4 inch down the body, the end points, a' and b', of the streamtube are determined by the limiting streamline and streamline that pass through a and b (Figure 43). Stretch is defined as the ratio of the distances a'b' and ab. This ratio proved to be fairly constant with respect to the initial height of the infinitesimal streamtube.

The stretch distributions are shown in Figures 44-46. The large bumps on the windward side are caused by a large skew in the flow direction due to the thinness of the boundary layer and the differences in the directions of the freestream and the boundary layer flow. A second bump occurs in the stretch curve after the skin friction lines have begun to converge. When a convergence line can be determined from the limiting streamline pattern, these figures show that the peak value of the second bump occurs at the convergence line for $\alpha = 10°$, Re = 12,000. It occurs just before the convergence line for the $\alpha = 15°$, Re = 12,000. For $\alpha = 10°$, Re = 300,000, there is a great deal of noise in the stretch distributions due to the oscillations in the computed flow direction at the first one or two grid points off the surface. These oscillations make it impossible to determine the circumferential location of peak stretch in Figure 46.

The stretch curves do not have sharp peaks near the convergence line. Instead, the peaks are fairly wide indicating that a large region of the flow is being pushed away from the surface. The magnitude of the stretch is very dependent upon the Reynolds number. For $\alpha = 10°$, the peak value of the stretch is approximately 8 times higher for Re = 300,000 than for Re = 12,000. There is a less pronounced dependency upon the angle of attack.

Two factors contribute to the stretching of the infinitesimal streamtube: the squeezing together of the streamlines and the drop in the skin friction magnitude. The skin friction magnitude decreases more rapidly on the windward side of the convergence line. Therefore, if the location of maximum stretch does not coincide with the convergence line, the maximum stretch should occur just a little to the windward side of the convergence line. This agrees with the observed behavior for $\alpha = 15°$.

In Figures 44-46, the peak values of the stretch do not coincide with the maximum $\partial(U_r/U_t)/\partial r$. This can be explained by the skew in the direction of the velocity near the surface. Because of this skew, the streamtube does not remain normal to the surface. Hence, only a portion of the stretch is used in forcing the fluid off the surface, and the location of the maximum streamtube stretching does not necessarily correspond to the location of the maximum flow angle.

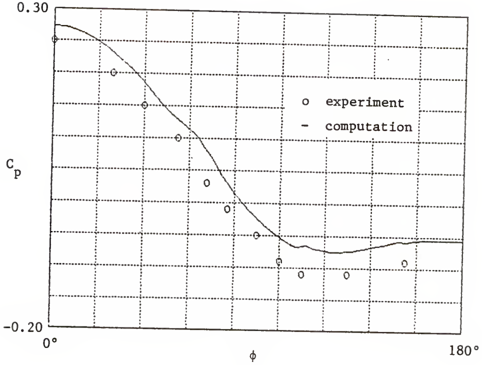

(a)

Figure 6. Static pressure coefficients for α = 15°, Re = 150,000, M_∞ = 1.98. a) 2.0 calibers aft of the nose.

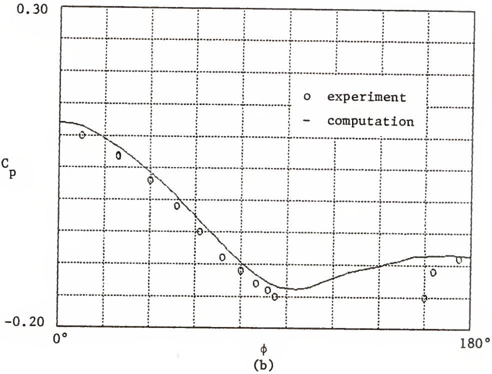

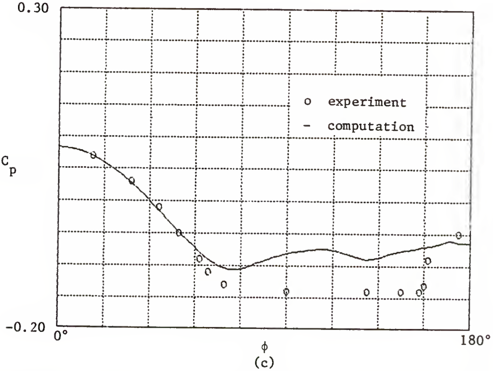

Figure 6. Continued; b) 3.0 calibers aft of the nose; c) 5.0 calibers aft of the nose.

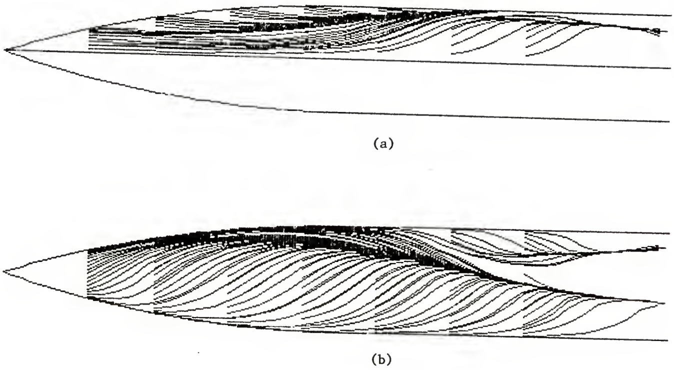

Figure 7. Limiting streamline pattern for $\alpha = 10°$, Re = 300,000. a) top view; b) side view.

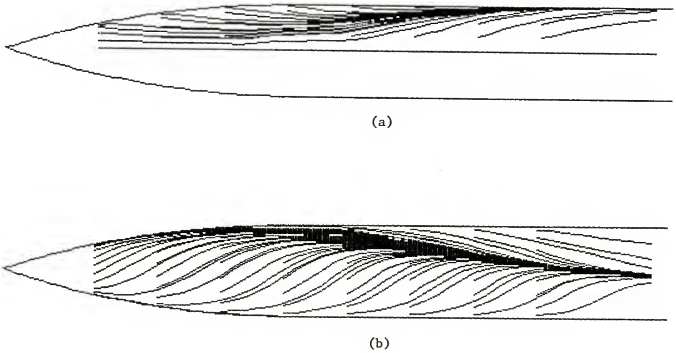

Figure 8. Limiting streamline pattern for α = 10°, Re = 12,000.
a) top view; b) side view.

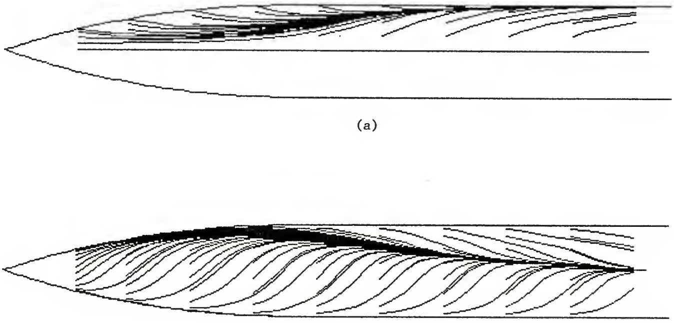

Figure 9. Limiting streamline pattern for α = 15°, Re = 12,000.
a) top view; b) side view.

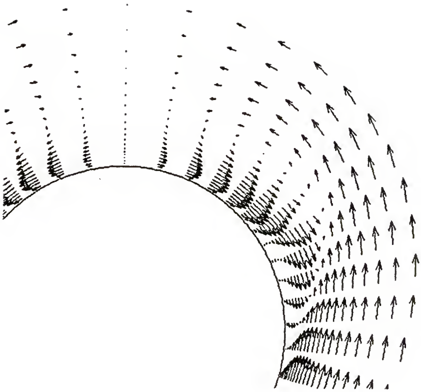

Figure 10. Crossflow velocities for $\alpha = 10°$, Re = 300,000. The crossflow plane is 5.0 calibers aft of the nose, and the distances from the body in the radial direction are multiplied by 4.0.

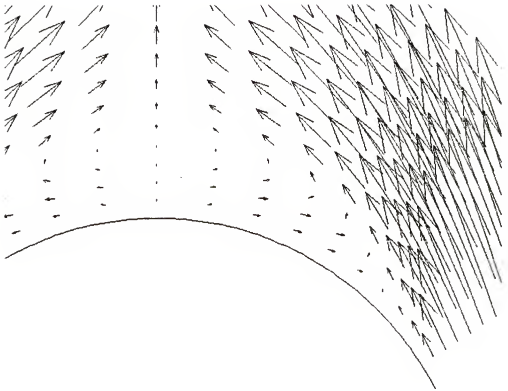

Figure 11. Crossflow velocities for α = 15°, Re = 12,000.
a) Crossflow plane at 2.97 calibers aft of the nose.

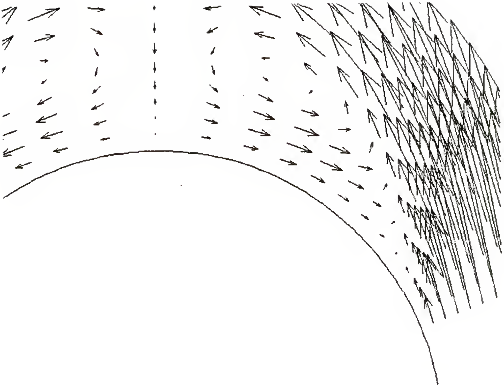

Figure 11. Continued; b) Crossflow plane at 3.64 calibers aft of the nose.

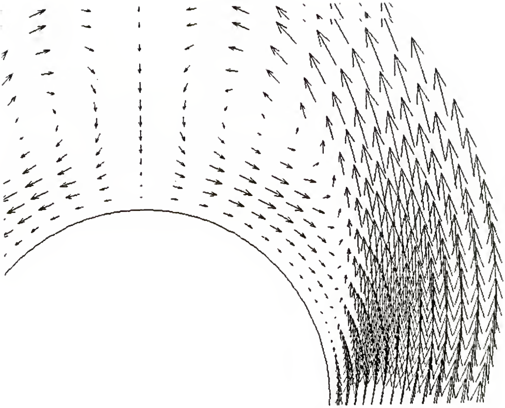

Figure 11. Continued; c) Crossflow plane at 4.97 calibers aft of the nose.

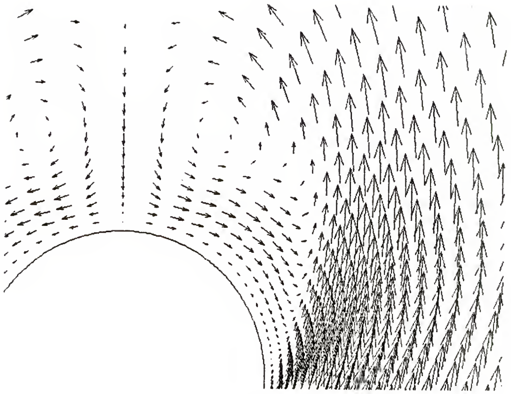

Figure 11. Continued; d) Crossflow plane at 6.31 calibers aft of the nose.

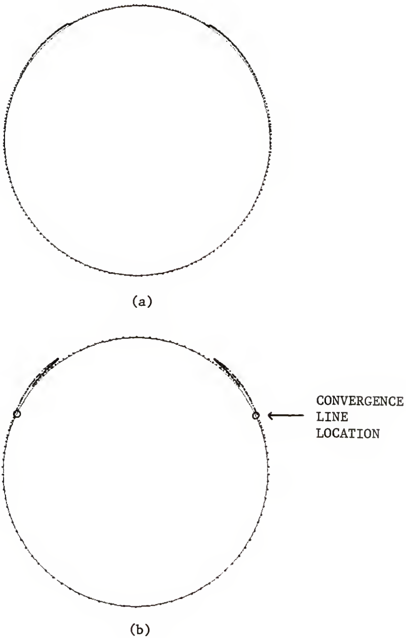

Figure 12. Crossflow cuts of an encircling streamtube for $\alpha = 10°$, Re = 300,000. The streamtube was started at 2.04 calibers aft of the nose as a circle with a radius 0.002 in. greater than the radius of the body. a) Crossflow plane at 2.97 calibers aft of the nose; b) Crossflow plane at 3.64 calibers aft of the nose.

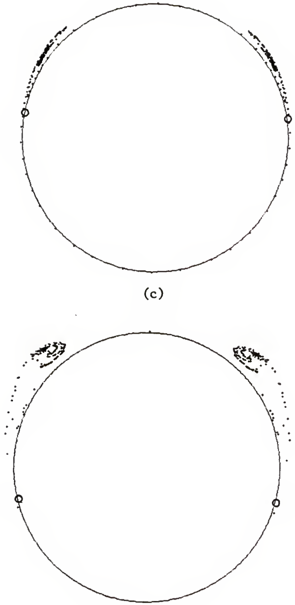

(c)

(d)

Figure 12. Continued; c) Crossflow plane at 4.31 calibers aft of the nose; d) Crossflow plane at 5.64 calibers aft of the nose.

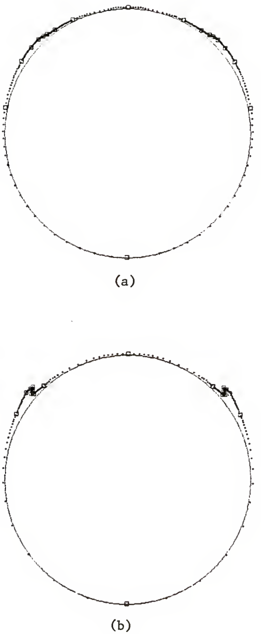

Figure 13. Crossflow cuts of an encircling streamtube for $\alpha = 10°$, Re = 12,000. The streamtube was started at 2.04 calibers aft of the nose as a circle with a radius 0.002 in. greater than the radius of the body. The squares represent streamlines started at 20° intervals. a) Crossflow plane at 3.64 calibers aft of the nose; b) Crossflow plane at 4.31 calibers aft of the nose.

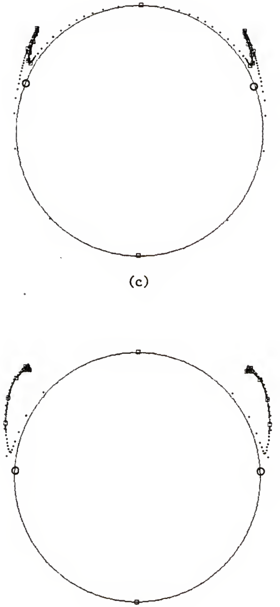

(c)

(d)

Figure 13. Continued; c) Crossflow plane at 4.97 calibers aft of the nose; d) Crossflow plane at 6.31 calibers aft of the nose.

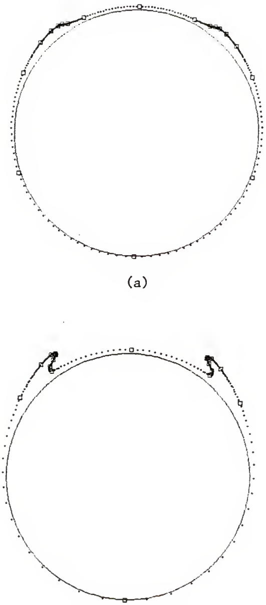

(a)

(b)

Figure 14. Crossflow cuts of an encircling streamtube for $\alpha = 15°$, Re = 12,000. The streamtube was started at 2.04 calibers aft of the nose as a circle with a radius 0.002 in. greater than the radius of the body. a) Crossflow plane at 2.97 calibers aft of the nose; b) Crossflow plane at 3.64 calibers aft of the nose.

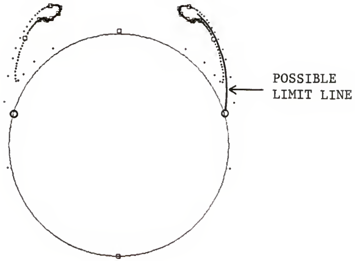

(c)

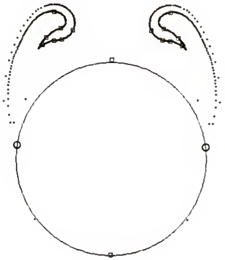

(d)

Figure 14. Continued; c) Crossflow plane at 4.97 calibers aft of the nose; d) Crossflow plane at 6.31 calibers aft of the nose.

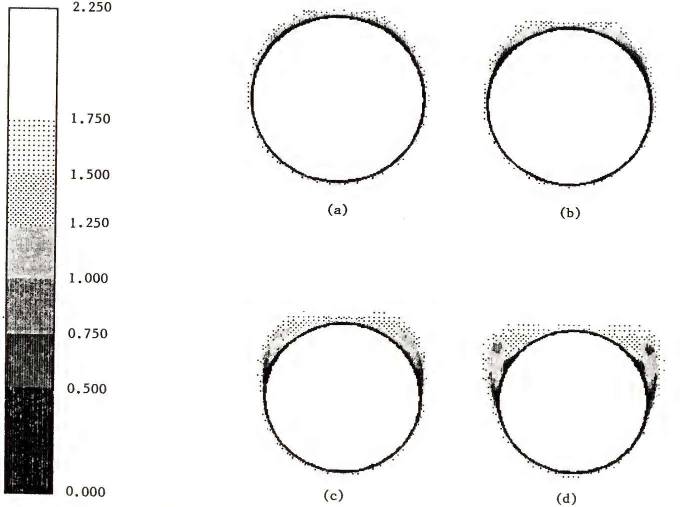

Figure 15. Mach number for $\alpha = 10°$, Re = 300,000. The distances from the body in the radial direction are multiplied by 4.0. a) Crossflow plane at 2.97 calibers aft of the nose; b) Crossflow plane at 3.64 calibers aft of the nose; c) Crossflow plane at 4.31 calibers aft of the nose; d) Crossflow plane at 4.97 calibers aft of the nose.

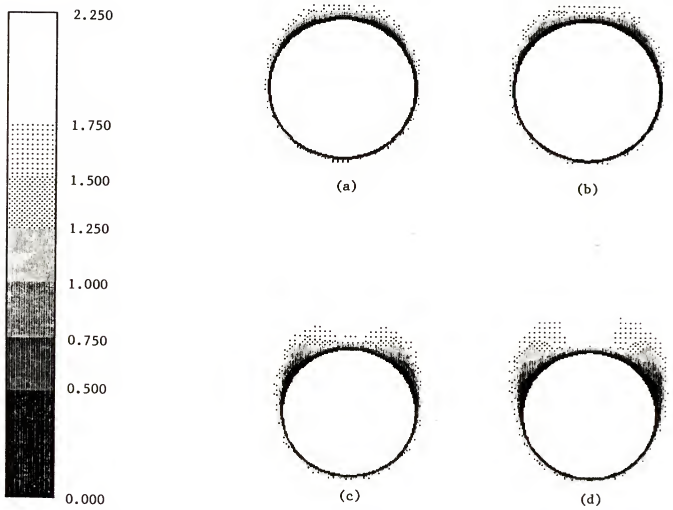

Figure 16. Mach number for $\alpha = 15°$, Re = 12,000. a) Crossflow plane at 2.97 calibers aft of the nose; b) Crossflow plane at 3.64 calibers aft of the nose; c) Crossflow plane at 4.97 calibers aft of the nose; d) Crossflow plane at 6.31 calibers aft of the nose.

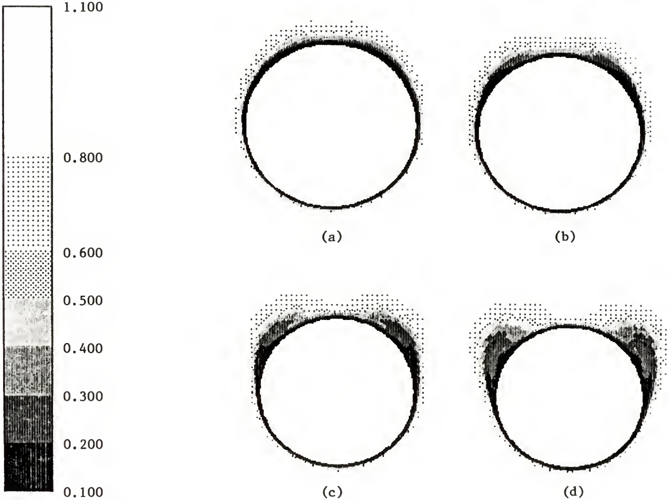

Figure 17. Pitot pressure for $\alpha = 10°$, Re = 300,000. The distances from the body in the radial direction are multiplied by 4.0. a) Crossflow plane at 2.97 calibers aft of the nose; b) Crossflow plane at 3.64 calibers aft of the nose; c) Crossflow plane at 4.31 calibers aft of the nose; d) Crossflow plane at 4.97 calibers aft of the nose.

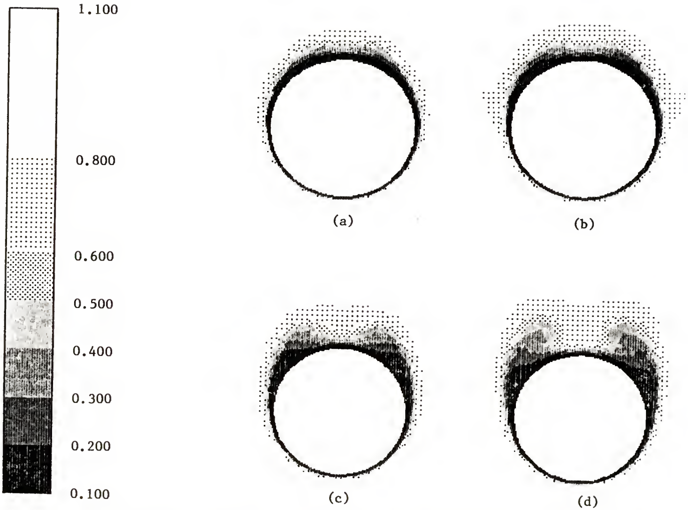

Figure 18. Pitot pressure for α = 15°, Re = 12,000. a) Crossflow plane at 2.97 calibers aft of the nose; b) Crossflow plane at 3.64 calibers aft of the nose; c) Crossflow plane at 4.97 calibers aft of the nose; d) Crossflow plane at 6.31 calibers aft of the nose.

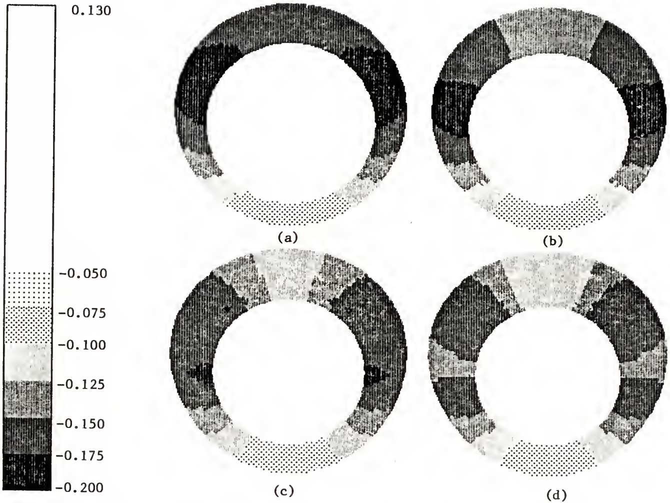

Figure 19. Static pressure coefficient for α = 10°, Re = 300,000. The distances from the body in the radial direction are multiplied by 4.0. a) Crossflow plane at 2.97 calibers aft of the nose; b) Crossflow plane at 3.64 calibers aft of the nose; c) Crossflow plane at 4.31 calibers aft of the nose; d) Crossflow plane at 4.97 calibers aft of the nose.

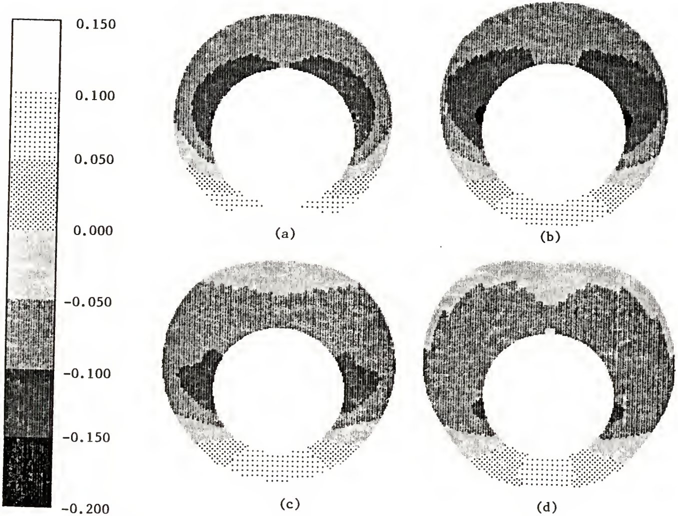

Figure 20. Static pressure coefficient for α = 15°, Re = 12,000. a) Crossflow plane at 2.97 calibers aft of the nose; b) Crossflow plane at 3.64 calibers aft of the nose; c) Crossflow plane at 4.97 calibers aft of the nose; d) Crossflow plane at 6.31 calibers aft of the nose.

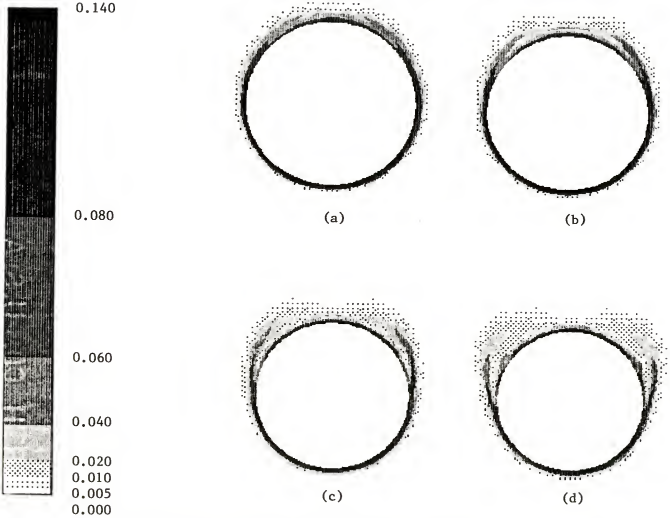

Figure 21. Vorticity magnitude for α = 10°, Re = 300,000. The distances from the body in the radial direction are multiplied by 4.0. a) Crossflow plane at 2.97 calibers aft of the nose. b) Crossflow plane at 3.64 calibers aft of the nose; c) Crossflow plane at 4.31 calibers aft of the nose; d) Crossflow plane at 4.97 calibers aft of the nose.

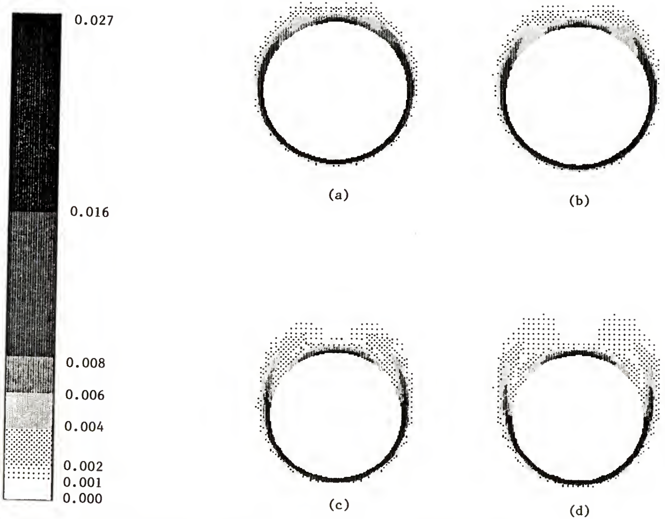

Figure 22. Vorticity magnitude for α = 15°, Re = 12,000. a) Crossflow plane at 2.97 calibers aft of the nose; b) Crossflow plane at 3.64 calibers aft of the nose; c) Crossflow plane at 4.97 calibers aft of the nose; d) Crossflow plane at 6.31 calibers aft of the nose.

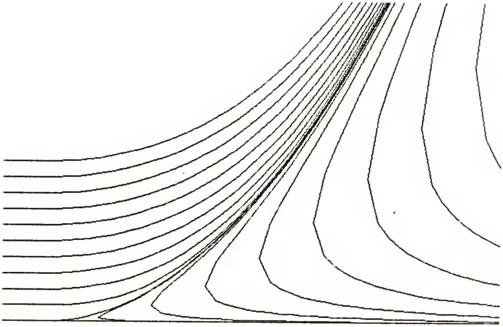

Figure 23. Nonsimple critical point that gives "tangential separation."

$$\frac{dy}{dz} = \frac{yz}{z - \frac{1}{2}y^2} \qquad y > 0$$

$$\frac{dy}{dz} = 0 \qquad y \leqslant 0$$

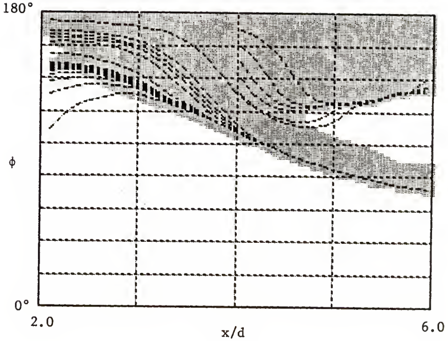

(a)

Figure 24. Reverse crossflow. The regions of reverse crossflow are shown in gray; x/d is the distance from the nose in calibers. a) α = 10°, Re = 300,000.

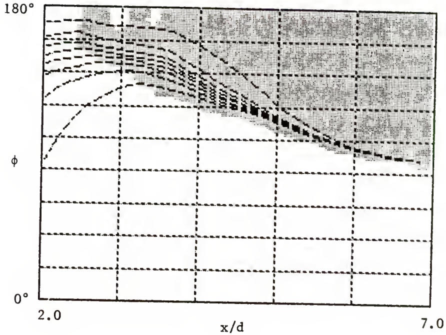

(b)

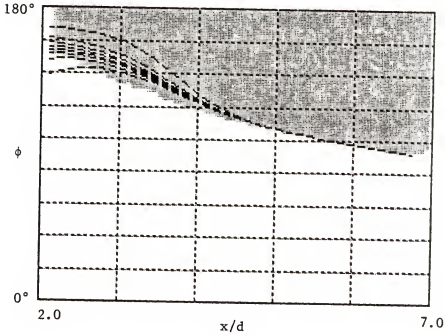

(c)

Figure 24. Continued; b) α = 10°, Re = 12,000; c) α = 15°, Re = 12,000.

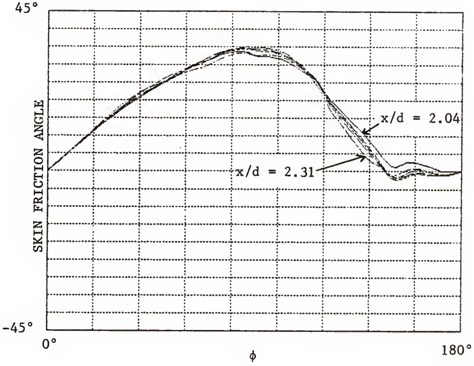

Figure 25. Skin friction angle, $\tan^{-1}(\tau_{\phi}/\tau_{ax})$, for $\alpha = 10°$, Re = 300,000. The skin friction angle is plotted for x/d = 2.04, 2.11, 2.17, 2.24, and 2.31 calibers aft of the nose.

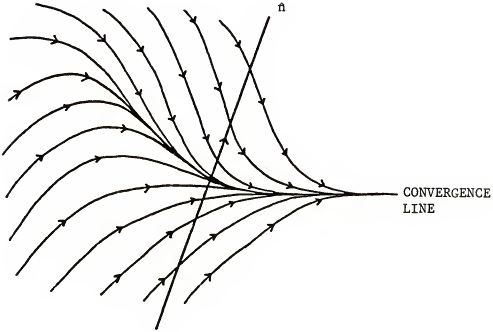

Figure 26. Definition of n̂, the normal to the convergence line.

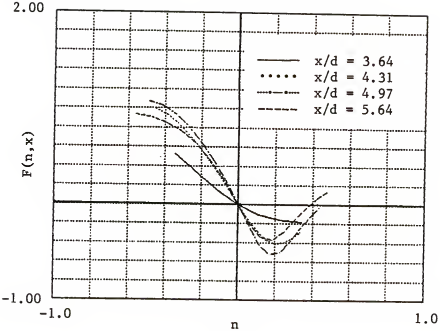

(a)

Figure 27. F(n,x). a) α = 10°, Re = 300,000.

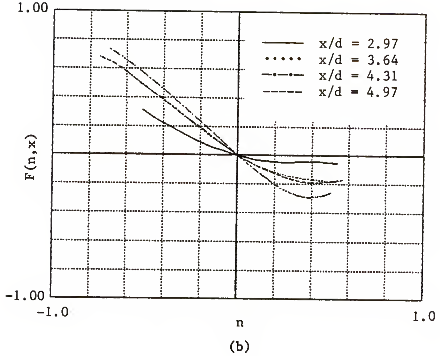

(b)

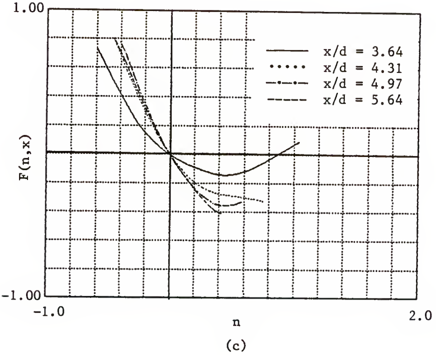

(c)

Figure 27. Continued; b) α = 10°, Re = 12,000; c) α = 15°, Re = 12,000.

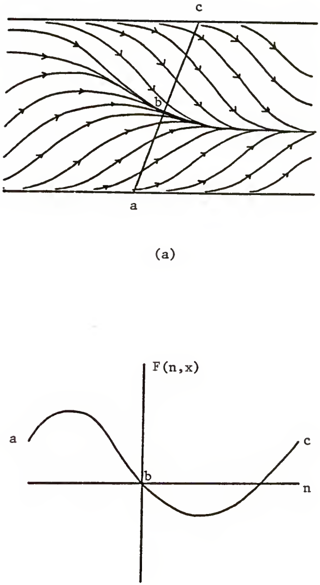

(a)

(b)

Figure 28. F(n,x) for a converging streamline pattern. a) Typical streamline pattern for crossflow separation; b) F(n,x) for the streamline pattern shown in (a).

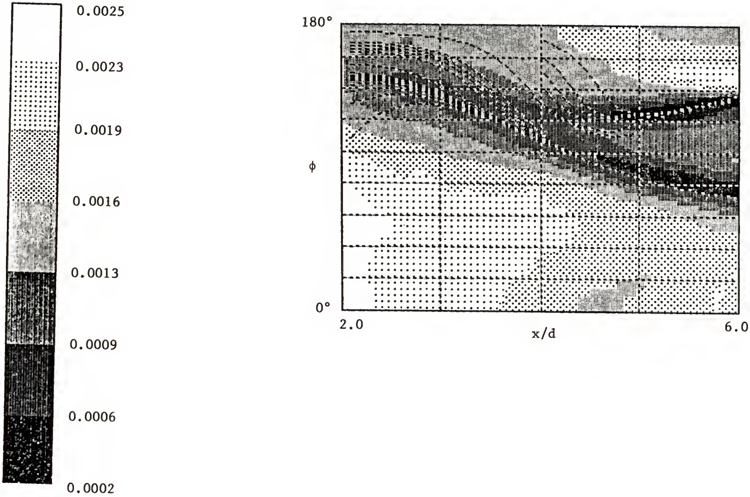

Figure 29. Skin friction magnitude for α = 10°, Re = 300,000. The distance from the nose, x/d, is in calibers.

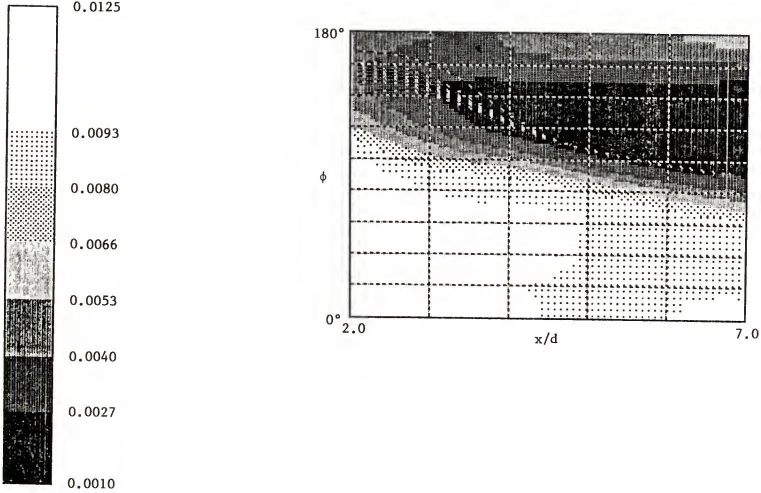

Figure 30. Skin friction magnitude for α = 15°, Re = 12,000. The distance from the nose, x/d, is in calibers.

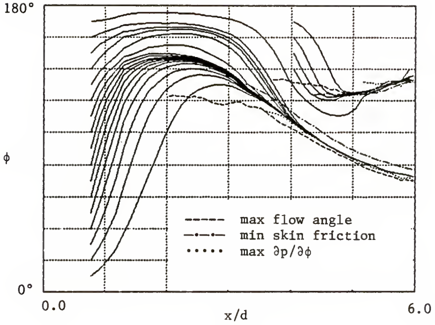

(a)

Figure 31. Circumferential minimums and maximums.
a) α = 10°, Re = 300,000.

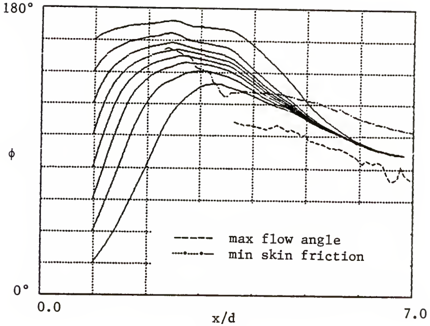

(b)

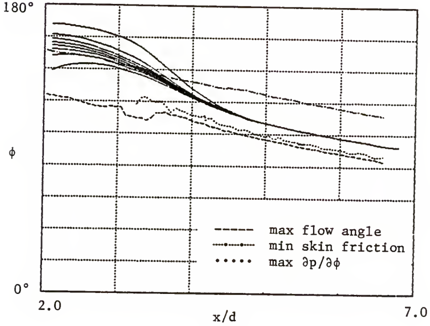

(c)

Figure 31. Continued; b) $\alpha = 10°$, Re = 12,000; c) $\alpha = 15°$, Re = 12,000.

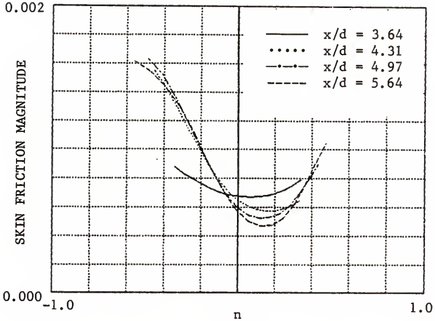

(a)

Figure 32. Skin friction magnitude. a) $\alpha = 10°$, Re = 300,000.

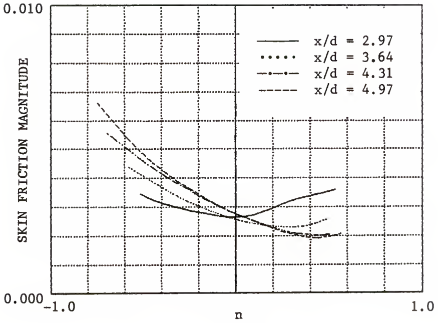

(b)

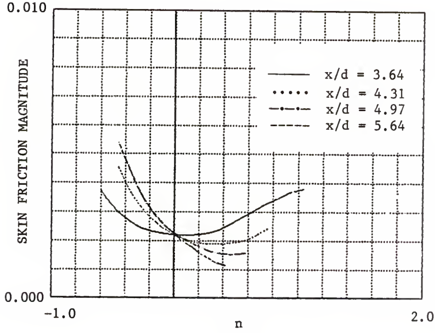

(c)

Figure 32. Continued; b) α = 10°, Re = 12,000; c) α = 15°, Re = 12,000.

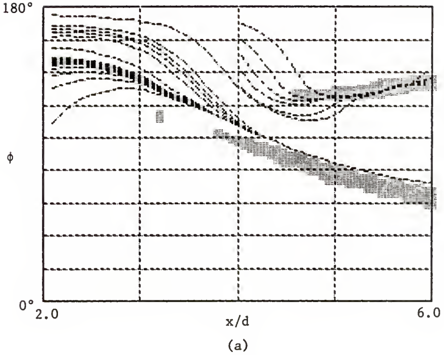

Figure 33. Negative $\partial|\vec{\omega}|/\partial r$. Regions of negative $\partial|\vec{\omega}|/\partial r$ are shown in gray; x/d is the distance from the nose in calibers. a) $\alpha = 10°$, Re = 300,000.

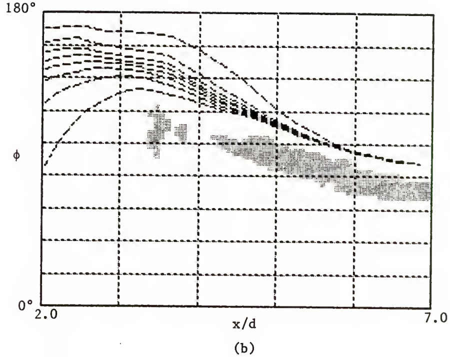

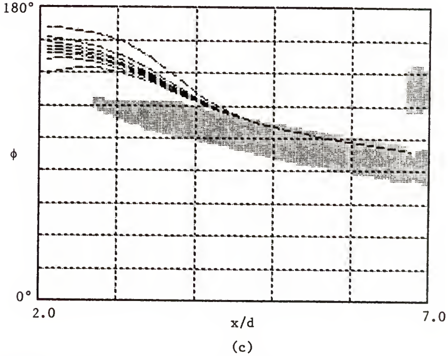

Figure 33. Continued; b) $\alpha = 10°$, Re = 12,000; c) $\alpha = 15°$, Re = 12,000.

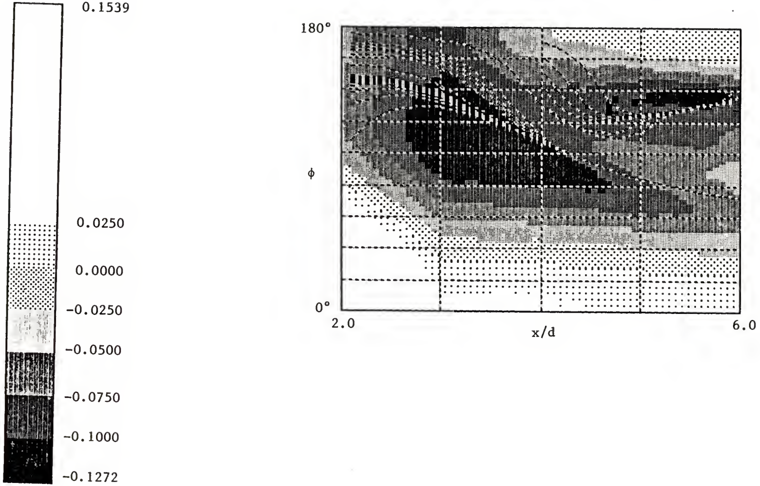

Figure 34. Static pressure coefficient for α = 10°, Re = 300,000. The distance from the nose, x/d, is in calibers.

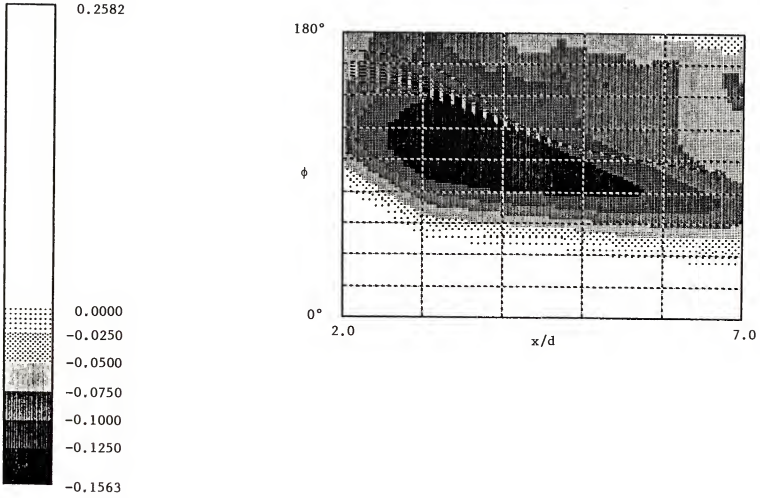

Figure 35. Static pressure coefficient for α = 15°, Re = 12,000. The distance from the nose, x/d, is in calibers.

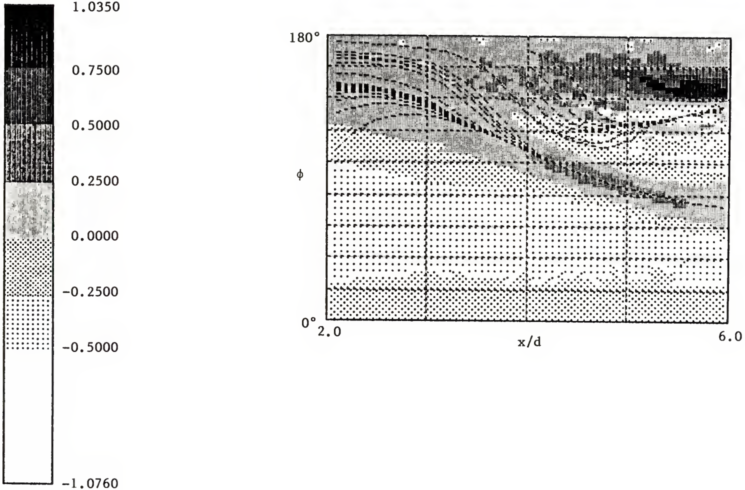

Figure 36. Pressure gradient, $\partial p/\partial \phi$, for $\alpha = 10°$, Re = 300,000. The distance from the nose, x/d, is in calibers.

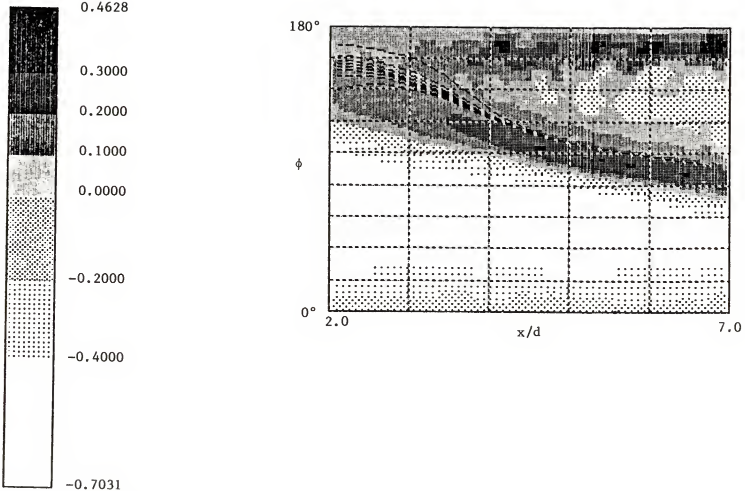

Figure 37. Pressure gradient, $\partial p/\partial\phi$, for $\alpha = 15°$, Re = 12,000. The distance from the nose, x/d, is in calibers.

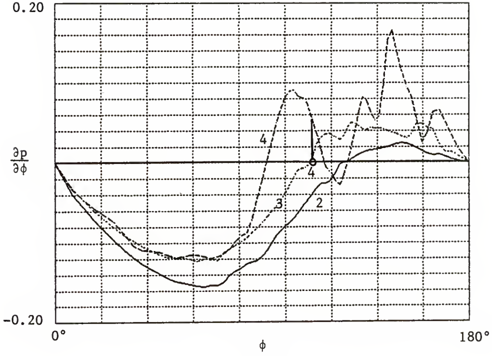

(a)

Figure 38. Pressure gradient, $\partial p/\partial \phi$. The circles represent the location of the convergence line. a) Pressure gradients at 2.0, 3.0, and 4.0 calibers aft of the nose for α = 10°, Re = 300,000.

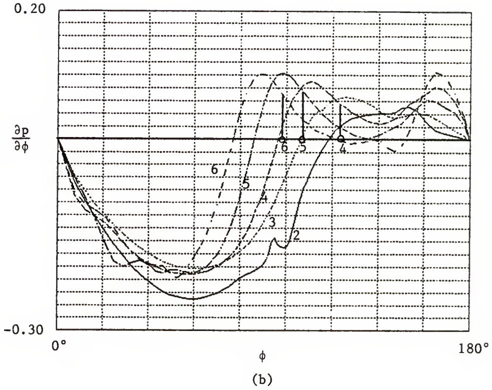

Figure 38. Continued; b) Pressure gradients at 2.0, 3.0, 4.0, 5.0, and 6.0 calibers aft of the nose for α = 15°, Re = 12,000.

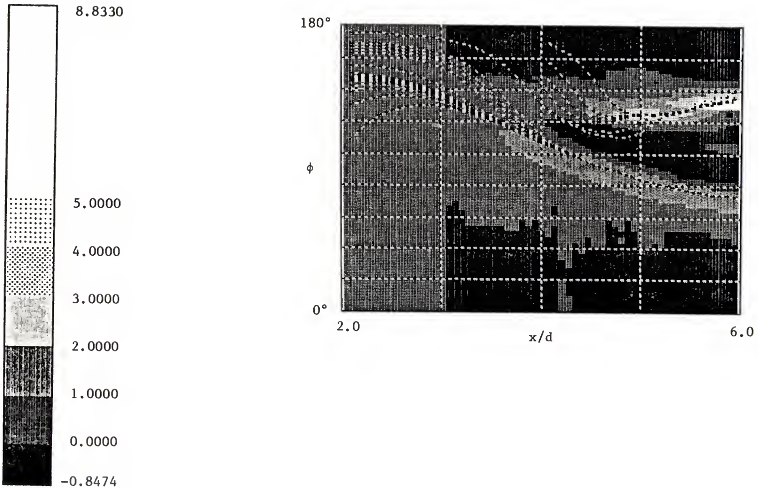

Figure 39. Derivative of the flow angle, $\partial(U_r/U_t)/\partial r$, for $\alpha = 10°$, Re = 300,000. The distance from the nose, x/d, is in calibers.

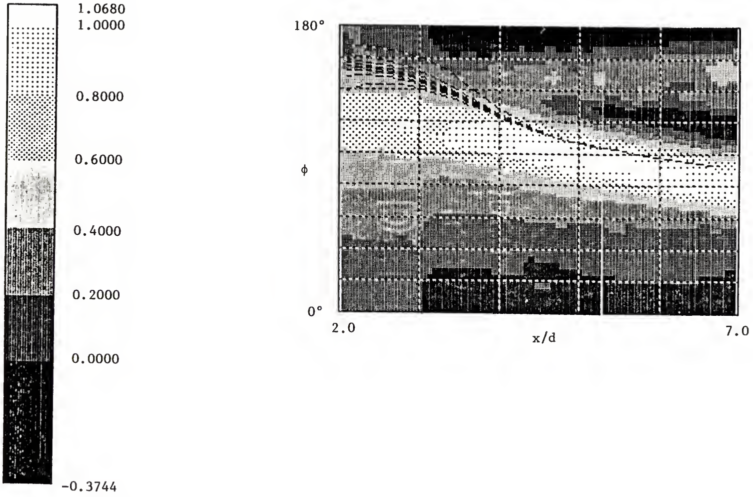

Figure 40. Derivative of the flow angle, $\partial(U_r/U_t)/\partial r$, for $\alpha = 15°$, Re = 12,000. The distance from the nose, x/d, is in calibers.

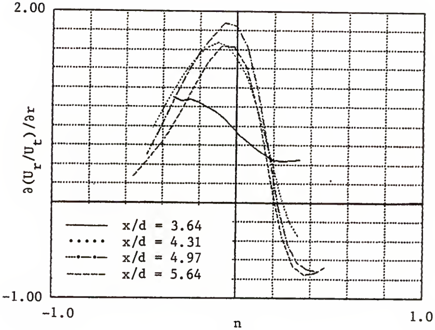

(a)

Figure 41. Flow angle derivative, $\partial(U_r/U_t)/\partial r$. a) α = 10°, Re = 300,000.

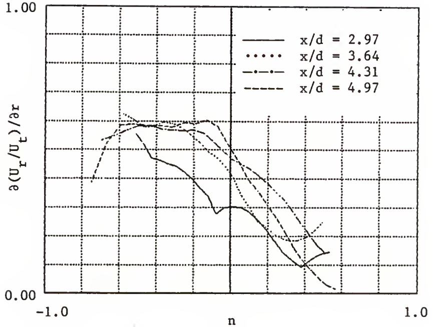

(b)

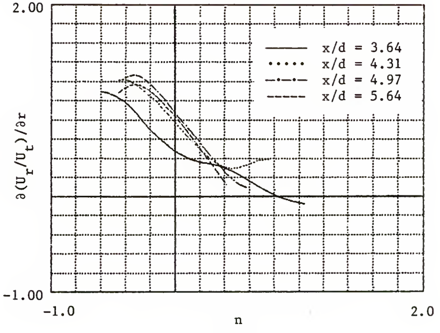

(c)

Figure 41. Continued; b) α = 10°, Re = 12,000; c) α = 15°, Re = 12,000.

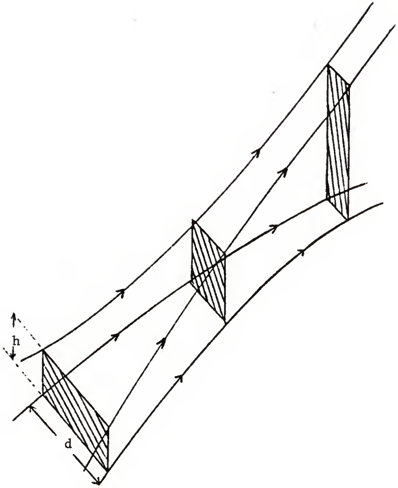

Figure 42. Streamtube. As the skin friction lines converge, the height of the streamtube increases, and flow is forced away from the surface.

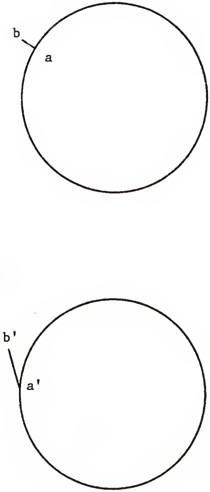

Figure 43. Stretch of an infinitesimal streamtube. a) Infinitesimal streamtube at x in. from the nose; b) Infinitesimal streamtube at x + 0.4 in. from the nose.

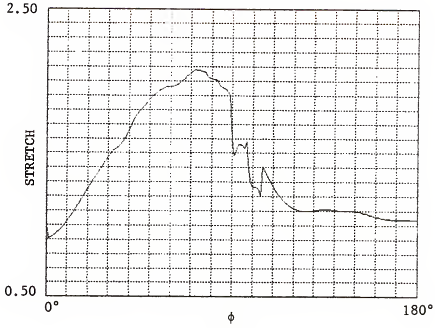

(a)

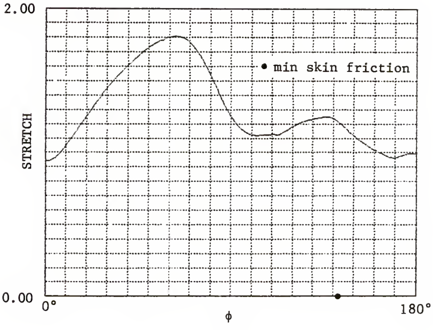

(b)

Figure 44. Stretch distributions for α = 10°, Re = 12,000. The stretch distributions are plotted for several starting locations, x/d. a) x/d = 1.64 calibers; b) x/d = 2.97 calibers.

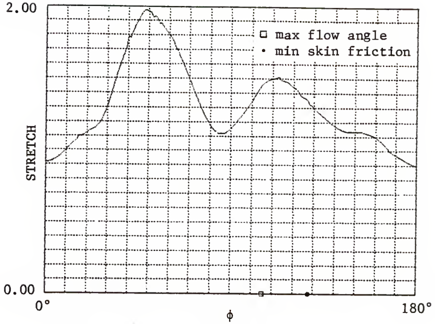

(c)

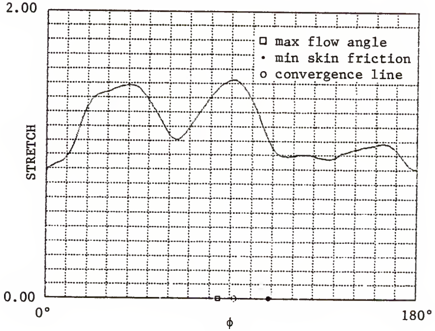

(d)

Figure 44. Continued; c) x/d = 4.3 calibers; d) x/d = 6.3 calibers.

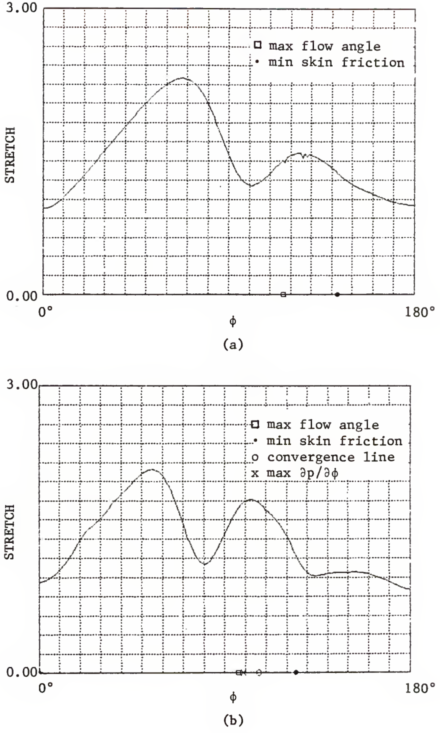

Figure 45. Stretch distributions for $\alpha = 15°$, Re = 12,000. a) $x/d = 3.04$ calibers; b) $x/d = 5.04$ calibers.

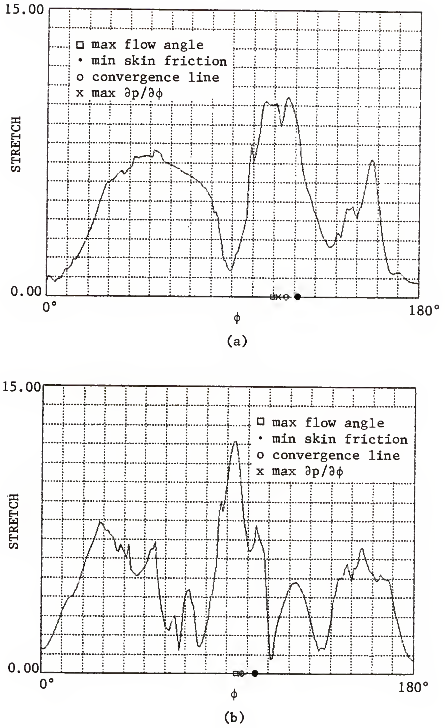

Figure 46. Stretch distributions for $\alpha = 10°$, Re = 300,000. a) $x/d = 3.70$ calibers; b) $x/d = 4.37$ calibers.

CHAPTER V
CONCLUSIONS

Crossflow separation on a tangent ogive resulted from a gradual squeezing of the fluid off the surface. There were no abrupt changes in the pressure, the vorticity, or the skin friction that indicated separation had occurred. Instead, these variables changed in a continuous manner as the crossflow separation developed.

The absence of abrupt changes in the flow variables made it impossible to determine where separation actually began unless a technique, such as the streamtube technique, was employed. The streamtube developed a bump as the skin friction lines began to converge. This bump became a fold which then elongated and rolled up as the distance from the nose increased. The onset of separation could be fairly well defined by the appearance of a fold in the streamtube.

The minimum and maximum pressure lines, the maximum pressure gradient lines, the minimum skin friction lines, and the maximum flow angle lines all paralleled the convergence line. None of these lines coincided with the convergence line, and the distances from the convergence line indicated that their offsets from the convergence line were true offsets and not the results of computational errors. Since the separation was fairly well established before the convergence line could be observed in the limiting streamline pattern, this parallel nature of the minimum and maximum lines appears to be a consequence of separation. It can be used to indicate that separation has occurred, but not where separation began.

The location of the convergence line came nearest to the location of maximum streamtube stretch and to the location of an inflection point in the limiting streamline direction. For stretching, the peak value was coincident with the convergence line for a Reynolds number of 12,000 and a 10° angle of attack. For a Reynolds number of 12,000 and a 15° angle of attack, the value was 3° to 4° to the windward side of the convergence line. The inflection point also appeared to occur at or near the convergence line.

Since the maximum flow angle, the maximum stretch, and the convergence lines did not coincide, it was not possible to define a circumferential separation location. It would be natural to define the separation location as the line at which the flow is leaving the surface at the largest angle or the line at which the stretching of the streamtubes is greatest. Neither definition, however, would agree with the usual definition of a separation line as the convergence line. For crossflow separation, it may be better to think in terms of a separation region which includes the convergence line rather than a single separation line. This interpretation would take into account the widening of the streamtube fold near the surface of the body, the broad peak in the stretch distribution, and the offset of the maximum flow angle from the peak stretch and convergence line. Furthermore, this interpretation of crossflow separation would also take into account the smooth behavior of the pressure, skin friction, and flow angle distributions.

REFERENCES

1. Wang, K.C., "On the Current Controversy of Unsteady Separation," AIAA Paper 83-0296, 1983.

2. Tobak, M., and Peake, D.J., "Topology of Two-Dimensional and Three-Dimensional Separated Flows," AIAA Paper 79-1480, 1979.

3. Tobak, M., and Peake, D.J., "Three-Dimensional Interactions and Vortical Flows with Empahsis on High Speeds," AGARDograph No. 252, 1980.

4. Andronov, A.A., Leontovich, E.A., Gordon, I.I., and Maier, A.G., Theory of Bifurcations on Dynamic Systems on a Plane, NASA TT F-556, 1971.

5. Andronov, A.A., Leontovich, E.A., Gordon, I.I., and Maier, A.G., Qualitative Theory of Second-Order Dynamic Systems, Wiley, New York, 1973.

6. Chapman, G.T., "Topological Classification of Flow Separation on Three-Dimensional Bodies," AIAA Paper 86-0485, 1986.

7. Zhang, H., "The Separation Criteria and Flow Behavior for Three Dimensional Steady Separated Flow," Translated from ACTA Aerodynamica Sinica, March 1985, pp. 1-12.

8. Chapman, G.T., Private communication.

9. Ta Phuoc, L., "Numerical Analysis of Unsteady Secondary Vortices Generated by an Impulsively Started Circular Cylinder," Journal of Fluid Mechanics, Vol. 100, Part 1, 1980, pp. 111-128.

10. Flegg, H.G., From Topology to Geometry, The English Universities Press Limited, London, 1974.

11. Legendre, R., "Lignes de Courant d'un Ecoulement Permanent: D'ecollement et Separation," Recherche Aerosptiale, Vol. 6, 1977, pp. 327-355.

12. Werle, H., "Separation on Axisymmetrical Bodies at Low Speeds," Recherche Aeronautique, No. 90, 1962, pp. 3-14.

13. Shanks, S.P., Srinivasan, G.R., and Nicolet, W.E., "AFWAL Parabolized Navier-Stokes Code: Formulation and User's Manual," Flow Simulations Inc., Sunnyvale, California, June 1982.

14. Schiff, L.B., and Steger, J.L., "Numerical Simulation of Steady Supersonic Viscous Flow," AIAA Paper 79-0130, 1979.

15. Rai, M.M., and Chaussee, D.S., "New Implicit Boundary Procedures: Theory and Applications," AIAA Paper 83-0123, 1983.

16. Jorgensen, L.H., and Perkins, E.W., "Investigations of Some Wake Vortex Characteristics of an Inclined Ogive-Cylinder at Mach Number 2," NACA Rept. 1371, 1958.

17. Intemann, G.A., "Experimental Investigation of the Location and Mechanism of Local Flow Separation on a 3-Caliber Tangent Ogive Cylinder at Moderate Angles of Attack," Master's Thesis, University of Florida, 1986.

18. Hirschel, E.H., and Kordulla, W., "Properties of Three-Dimensional Separation Lines," Z. Flugwiss, Vol. 5, April 1980, pp. 295-307.

19. Lighthill, M.J., "Attachment and Separation in Three-Dimensional Flow," Laminar Boundary Layers, edited by L. Rosenhead II, Oxford University Press, Oxford, 1963, pp. 72-82.

BIOGRAPHICAL SKETCH

Leslie Anne Nelson Yates was born in Waterloo, Iowa, in 1954. She graduated from South Eugene High School in Eugene, Oregon, in 1972, received her B.A. in physics from New College in Sarasota, Florida, in 1976, and studied physics at the State University of New York from 1976-1979. She married Christopher Yates in 1979. She earned her M.S. in 1983 and her Ph.D. in 1986 from the University of Florida Department of Engineering Sciences.

I certify that I have read this study and that in my opinion it conforms to acceptable standards of scholarly presentation and is fully adequate, in scope and quality, as a dissertation for the degree of Doctor of Philosophy.

Mark H. Clarkson

Mark H. Clarkson, Chairman
Professor of Engineering Sciences

I certify that I have read this study and that in my opinion it conforms to acceptable standards of scholarly presentation and is fully adequate, in scope and quality, as a dissertation for the degree of Doctor of Philosophy.

Knox T. Millsaps
Professor of Engineering Sciences

I certify that I have read this study and that in my opinion it conforms to acceptable standards of scholarly presentation and is fully adequate, in scope and quality, as a dissertation for the degree of Doctor of Philosophy.

Joseph L. Hammack

Joseph L. Hammack
Professor of Engineering Sciences

I certify that I have read this study and that in my opinion it conforms to acceptable standards of scholarly presentation and is fully adequate, in scope and quality, as a dissertation for the degree of Doctor of Philosophy.

Richard L Fearn

Richard L. Fearn
Professor of Engineering Sciences

I certify that I have read this study and that in my opinion it conforms to acceptable standards of scholarly presentation and is fully adequate, in scope and quality, as a dissertation for the degree of Doctor of Philosophy.

Bernard M. Leadon
Professor of Engineering Sciences

I certify that I have read this study and that in my opinion it conforms to acceptable standards of scholarly presentation and is fully adequate, in scope and quality, as a dissertation for the degree of Doctor of Philosophy.

David M Locke

David M. Locke
Associate Professor of English

This dissertation was submitted to the Graduate Faculty of the College of Engineering and to the Graduate School and was accepted as partial fulfillment of the requirements for the degree of Doctor of Philosophy.

August 1986

Hubert A. Bevis

Dean, College of Engineering

Dean, Graduate School